CONFIDENTIAL

NACA

RESEARCH MEMORANDUM

WIND-TUNNEL MEASUREMENTS OF THE DYNAMIC CROSS DERIVATIVE $C_{l_r} - C_{l_{\dot{\beta}}}$ (ROLLING MOMENT DUE TO YAWING VELOCITY AND TO ACCELERATION IN SIDESLIP) OF THE DOUGLAS D-558-II AIRPLANE AND ITS COMPONENTS AT SUPERSONIC SPEEDS INCLUDING DESCRIPTION OF THE TECHNIQUE

By William B. Boatright

Langley Aeronautical Laboratory
Langley Field, Va.

CLASSIFIED DOCUMENT

NATIONAL ADVISORY COMMITTEE FOR AERONAUTICS

WASHINGTON

November 3, 1955

CONFIDENTIAL

[redacted]

NATIONAL ADVISORY COMMITTEE FOR AERONAUTICS

RESEARCH MEMORANDUM

WIND-TUNNEL MEASUREMENTS OF THE DYNAMIC CROSS DERIVATIVE $C_{l_r} - C_{l_{\dot{\beta}}}$ (ROLLING MOMENT DUE TO YAWING VELOCITY AND TO ACCELERATION IN SIDESLIP) OF THE DOUGLAS D-558-II AIRPLANE AND ITS COMPONENTS AT SUPERSONIC SPEEDS INCLUDING DESCRIPTION OF THE TECHNIQUE

By William B. Boatright

SUMMARY

A technique is described and results are presented of wind-tunnel forced-oscillation tests of a model of the Douglas D-558-II research airplane which was instrumented to obtain the dynamic cross derivative $C_{l_r} - C_{l_{\dot{\beta}}}$ (rolling moment due to yawing velocity and to acceleration in sideslip) and the static derivative C_{l_β} (rolling moment due to sideslip). The tests were conducted for the complete configuration at Mach numbers 1.62, 1.94, and 2.41 for an angle-of-attack range from 0° to about 8°. Component tests of the body-tail and the body-wing were made at Mach numbers 1.62 and 2.41.

It is shown that the wing-body contribution to $C_{l_r} - C_{l_{\dot{\beta}}}$ is predominant for this airplane as compared with the body-tail contribution and produces a large negative value of $C_{l_r} - C_{l_{\dot{\beta}}}$. This means that the moment associated with this derivative would produce a negative rolling moment when the airplane is yawing to the right, although in a static condition at a positive angle of attack, a positive rolling moment is produced by a positive angle of yaw of the wing (C_{l_β} is negative).

Results of sample calculations of the period and damping of the full-scale airplane, although not conclusive because of the inadequate number of flight conditions investigated, are included in an attempt to assess the importance of the large negative values of the cross derivative that were measured in this investigation, as compared with the positive values of this derivative previously estimated.

[redacted]

INTRODUCTION

Flight experience has indicated that many stability problems must be defined and solved in order to control current supersonic aircraft throughout the supersonic speed ranges now being attained. It has further become evident that due to increased weight and wing loading of the aircraft, the larger proportion of the weight being concentrated in the fuselage, and the attainment of higher altitudes, the dynamic characteristics of the aircraft have increased in importance and should be considered in the early stages of design. Reliable estimates of the dynamic lateral stability derivatives are important to assess the effect of these derivatives on the total airplane stability. Subsonic wind-tunnel studies (refs. 1 to 4) have demonstrated the value of special wind-tunnel techniques in measuring some of the dynamic derivatives. However, little is known of the dynamic derivatives at supersonic speeds with the possible exception of the damping-in-roll derivative, and in this case only at zero angle of attack.

Some of the limited knowledge concerning the dynamic derivatives at supersonic speeds has been obtained from reference 5 which presents a supersonic wind-tunnel study of the lateral derivatives of a generalized wing-body model using a special two-degree-of-freedom wind-tunnel technique. Also lateral stability data obtained from free flight rocket model tests to a Mach number high as 1.15 are presented in reference 6. The damping-in-roll derivative C_{l_p} has been investigated both in supersonic wind tunnels and with rocket tests, but experimental information on the contribution to this derivative of airplane components (wing, body, and tail) in combination is only beginning to receive attention.

Reference 7 reviews a method for estimating the lateral dynamic derivatives if the sideslip derivatives, such as are presented in references 8 and 9 for the Douglas D-558-II airplane, are known, but the necessary approximations limit the confidence with which the method can be used. Reference 10 indicates that the side force due to rolling and yawing C_{Y_p} and C_{Y_r} have a negligible effect on the period and damping of an airplane, at least for the configurations investigated. Reference 11 indicates that the lateral acceleration derivatives can be important. It thus appears that information enabling a reliable estimate of the derivatives associated with (a) yawing moment due to rolling C_{n_p}, (b) yawing moment due to yawing C_{n_r}, (c) yawing moment due to acceleration in sideslip $C_{n_{\dot{\beta}}}$, (d) side force due to rolling C_{Y_p}, and (e) the rolling moment due to yawing and acceleration in sideslip C_{l_r} and $C_{l_{\dot{\beta}}}$ are needed. It is the purpose of the present investigation to furnish data on the latter two of these derivatives in combination. Although

[redacted]

their separate effects were not obtained, calculations of the period and damping assuming different proportions of one to the other for a given experimentally measured value of their difference were made.

The tests of this investigation furnish data for the complete configuration of the D-558-II airplane configuration at Mach numbers of 1.62, 1.94, and 2.41 and component breakdown tests at Mach numbers 1.62 and 2.41. Tests were conducted at angles of attack from 0° to about 8°. Finely ground salt transition strips were located near the leading edges of the wing, the vertical and horizontal tails, and near the nose of the body in order that the boundary-layer effects at high Reynolds numbers might be more closely simulated.

The technique is discussed in detail since the unexpected results require that the reader have an adequate knowledge of the technique in order to assess properly the validity of the data.

SYMBOLS

A	wing aspect ratio, b^2/S
b	wing span, ft
Δh	distance on film from zero reference to ψ trace, in.
i	wing-incidence angle, deg
I_{xz}	product of inertia of model with respect to xz-plane, slug-ft^2
I_{yz}	product of inertia of model with respect to yz-plane, slug-ft^2
k_{x_o}	radius of gyration in roll of full-scale airplane about principal longitudinal axis of inertia, ft
k_{z_o}	radius of gyration in yaw of full-scale airplane about principal normal axis of inertia, ft
L	rolling moment, ft-lb
L_β	rate of change of rolling moment with sideslip angle, $\partial L/\partial\beta$, ft-lb/radians
$L_{\beta\text{-}B} = L_\beta$	referenced to body axis
$L_{\dot{\beta}}$	rate of change of rolling moment with acceleration in sideslip, $\partial L/\partial\dot{\beta}$, ft-lb-sec/radians

[redacted]

$L_{\dot{\beta}-B} = L_{\dot{\beta}}$ referenced to body axis

$L_{\dot{\psi}}$ rate of change of rolling moment with yawing angular velocity, $\partial L/\partial \dot{\psi}$, ft-lb-sec/radians

$L_{\dot{\psi}-B} = L_{\dot{\psi}}$ referenced to body axis

$L_{\ddot{\psi}}$ rate of change of rolling moment with yawing angular acceleration, $\partial L/\partial \ddot{\psi}$, ft-lb-sec^2/radians

$L_{\phi-B}$ rate of change of rolling moment with roll angle (ϕ referenced to body axis), $\partial L/\partial \phi_B$, ft-lb/radians

$L_{\dot{\phi}-B}$ rate of change of rolling moment with rolling angular velocity ($\dot{\phi}$ referenced to body axis), $\partial L/\partial \dot{\phi}_B$ ft-lb-sec/radians

L_t total rolling moment as indicated by strain gage, ft-lb

M Mach number

m.a.c. mean aerodynamic chord

N yawing moment, ft-lb

N_β rate of change of yawing moment with sideslip angle, $\partial N/\partial \beta$, ft-lb/radians

$N_{\dot{\beta}}$ rate of change of yawing moment with acceleration in sideslip, $\partial N/\partial \dot{\beta}$, ft-lb-sec/radians

$N_{\dot{\psi}}$ rate of change of yawing moment with yawing angular velocity, $\partial N/\partial \dot{\psi}$, ft-lb-sec/radians

p rolling angular velocity, radians/sec

P period of oscillation, sec

q dynamic pressure, $\frac{1}{2}\rho V^2$

r yawing angular velocity, radians/sec

R distance from mirror on model to film in drum camera

Re Reynolds number

[redacted]

S	wing area, sq ft
t	time, sec
T	torque about x-axis, ft-lb
$T_{1/2-1}$	time to damp to 1/2 amplitude of spiral mode of motion, sec
$T_{1/2-2}$	time to damp to 1/2 amplitude of roll mode of motion, sec
$T_{1/2-3}$	time to damp to 1/2 amplitude of oscillatory mode of motion, (- value denotes time to double amplitude), sec
V	free stream velocity, ft/sec
W	weight of airplane, lb
x,y,z	longitudinal, lateral, and normal axes, respectively, of stability axis system
α	angle of attack, deg or radians
β	angle of sideslip, deg or radians
$\dot{\beta}$	rate of change of sideslip angle with time, $\partial\beta/\partial t$, deg/sec or radians/sec
ϵ	angle between fuselage center line and principal axis, deg
ψ	angle of yaw, deg or radians
$\psi_B = \psi$	referenced to body axis
$\dot{\psi}$	yawing angular velocity, $\partial\psi/\partial t$, deg/sec or radians/sec
$\dot{\psi}_B = \dot{\psi}$	referenced to body axis
$\ddot{\psi}$	yawing angular acceleration, $\partial^2\psi/\partial t^2$, deg/sec^2 or radians/sec^2
ϕ_B	angle of roll (referenced to body axis), radians
$\dot{\phi}_B$	rolling angular velocity (referenced to body axis), radians/sec
C_l	rolling-moment coefficient, L/qSb

[redacted]

$C_{l_\beta} = \frac{\partial C_l}{\partial \beta}$

$C_{l_{\dot{\beta}}} = \frac{\partial C_l}{\partial \frac{\dot{\beta} b}{2V}}$

$C_{l_{\dot{\beta}}'} = \frac{\partial C_l}{\partial \dot{\beta}}$

$C_{l_p} = \frac{\partial C_l}{\partial \frac{pb}{2V}}$

$C_{l_r} = \frac{\partial C_l}{\partial \frac{rb}{2V}}$

$C_{l_{\dot{\psi}}} = \frac{\partial C_l}{\partial \dot{\psi}}$

C_n yawing-moment coefficient, N/qSb

$C_{n_\beta} = \frac{\partial C_n}{\partial \beta}$

$C_{n_{\dot{\beta}}} = \frac{\partial C_n}{\partial \frac{\dot{\beta} b}{2V}}$

$C_{n_p} = \frac{\partial C_n}{\partial \frac{pb}{2V}}$

$C_{n_r} = \frac{\partial C_n}{\partial \frac{rb}{2V}}$

C_Y side-force coefficient, Y/qS

$C_{Y_\beta} = \frac{\partial C_Y}{\partial \beta}$

[redacted]

$$C_{Y_{\dot{\beta}}} = \frac{\partial C_Y}{\partial \frac{\dot{\beta} b}{2V}}$$

$$C_{Y_p} = \frac{\partial C_Y}{\partial \frac{pb}{2V}}$$

$$C_{Y_r} = \frac{\partial C_Y}{\partial \frac{rb}{2V}}$$

APPARATUS

Tunnel

The Langley 9-inch supersonic tunnel is a closed-circuit continuously operating wind tunnel in which the pressure, temperature, and humidity of the enclosed air can be regulated. Different test Mach numbers can be obtained by interchangeable nozzle blocks which form a test section about 9 inches square.

Model and Model Support

The 1/72-scale model (without canopy) of the Douglas D-558-II airplane, shown in figure 1, was fabricated of steel and fibre-glass plastic so that it would house an internal rolling-moment strain-gage balance. Interchangeable nose sections which fastened rigidly to the balance and wing and tail sections which always had clearance between them and the balance or sting support were designed so that either the complete configuration, the body wing, or the body tail could be tested separately. Provision for changing angle of attack of the model was made by the series of 1/8-inch-diameter holes in the disc of the rear of the sting into which pins could be inserted and mated with matching holes in the model support. Figure 2 is a photograph illustrating the method of supporting the model in the tunnel in an inverted position. The swept-back struts formed a rigid triangular truss in front view and other than the slightly modified tail section to allow for a small gusset on the sting there was no support interference on the model. A shaft integral with the model support penetrated the top nozzle of the tunnel. This shaft defined the pivot point of the yawing oscillation and was designed at a mean center-of-gravity location of the full-scale airplane which corresponded almost exactly to the actual center of gravity of the model.

Oscillating Equipment

The model was oscillated in yaw from -12.5° to +12.5°. Of this cycle ±7° was at constant angular velocity. The remaining portion of the cycle was at constant angular acceleration in order to keep inertia loads which might interact with the balance to a minimum. This prescribed motion was accomplished by forcing a rocker arm, to which the shaft through the top of the tunnel was keyed, to ride on a cam. The photograph, figure 3, shows a view of the oscillating apparatus although the cam is obscured by the flywheel. The flywheel was keyed to the same shaft as the cam and its purpose was to maintain constant rotational speed of the cam. An additional aid in providing constant cam rotational speed was the dummy spring loaded rocker arm whose force on the cam opposed the force produced by the rocker arm to which the model was keyed. A 3/4-horsepower electric motor coupled through a gear box, also obscured by the flywheel, motivated the cam. A variac between the power supply and the electric motor permitted rotation of the cam at various speeds thus changing the frequency of oscillation of the model. A tachometer, whose signal was obtained from a small generator directly coupled to the cam shaft, permitted the operator to observe the approximate frequency of the oscillation of the model.

Recording Equipment

A specially designed drum camera using 9-inch-wide roll film, such as is used in a K-19 or K-22 aerial photograph camera, was mounted on the side of the tunnel. A light signal from a small 1/16-inch-diameter mirror on the model made a trace denoting the history of the angular position of the model on the film when both the drum and model were in motion. Simultaneously, the amplified strain-gage signal was fed to an oscillograph whose light trace exposed the film from the opposite side and denoted the history of the rolling moment of the model. Figure 4 is a general view of the drum camera mounted in position on the side of the tunnel with auxiliary equipment on a table in the foreground. Figure 5 is a close-up view of the drum camera. The circular drum cover which can be seen in figure 5 inclosed a 30-inch-diameter revolving drum, made of Plexiglass and aluminum, to which the film was clipped. The film was precut to the correct length (about 90 inches) and at the oscillation frequencies and drum speeds that were used permitted a record of about 5 cycles to be printed for each test. Synchronized automatic shutters were a design feature of the drum camera so that when the model oscillating frequency and the drum speed had been adjusted to their desired values, a manual switch was activated and the shutter opened automatically at the start of the film and closed after one revolution of the drum.

The oscillograph apparatus mounted on a table inside the drum consisted of two active galvanometer elements and two minute stationary

reference mirrors. One of the active galvanometer elements recorded the strain-gage signal after it had been amplified by a Carrier-Amplifier. The other active galvanometer element was used as a timing light and obtained its signal from a conventional electrical oscillator. A switching arrangement permitted the signal from this oscillator to be fed either into the galvanometer element during a test or into a Stroboconn immediately preceding a test in order to accurately set the oscillator output at the desired frequency.

Figure 6 is a sketch illustrating a general view of the orientation of the model, drum camera, and the paths of the various light beams used in recording the data. The oscillograph light source was a standard straight-line filament-type bulb. The light source for making the angular position trace which reflected off the model mirror was a mercury arc air-cooled light source. A similar light source was mounted on a calibrated scale 80 inches from the opposite side of the model. A 1/16-inch-diameter mirror recessed into the opposite side of the model from the drum camera reflected the light from this source onto the calibrated scale and was used during a static test for accurately positioning the model in the tunnel.

TESTS

General Considerations

The torque about the x-axis of a rigid body performing one-degree-of-freedom rotation about a z-axis (ψ varying with time) is

$$T_x = -I_{xz}\ddot{\psi} - I_{yz}\dot{\psi}^2 \tag{1}$$

For a wind-tunnel model where the angle of yaw ψ is inherently equal to the negative of the angle of sideslip β and a strain gage resists the total moment about the x-axis with a moment L_t, the equation of motion can be expressed as

$$L_t - L_\beta\psi + \left(L_{\dot{\psi}} - L_{\dot{\beta}}\right)\dot{\psi} = \left(-I_{xz} - L_{\ddot{\psi}}\right)\ddot{\psi} - I_{yz}\dot{\psi}^2 \tag{2}$$

[redacted]

For a model which is symmetrical about the xz-plane, $I_{yz} = 0$. If the model moves with constant angular velocity, $\ddot{\psi} = 0$; and the equation of motion becomes simply

$$L_t - L_\beta \psi = -\left(L_{\dot{\psi}} - L_{\dot{\beta}}\right)\dot{\psi} \tag{3}$$

It is thus apparent that the difference between the dynamic measurement of the rolling moment and the static measurement furnish a means of measuring the combined cross derivative $C_{l_r} - C_{l_{\dot{\beta}}}$ when $\dot{\psi}$ is known, or at $\psi = 0$ the strain gage will read the moment associated with this cross derivative directly.

The previously mentioned equations apply without qualification to the tests of this investigation at $\alpha = 0^\circ$. At angles of attack other than 0°, a mixed system of axes exists. The motion was prescribed in the stability axis system whereas the rolling moment was measured about the body axis. This measured rolling moment is composed of the following aerodynamic terms when referred to the stability axis: $N_\beta \psi \sin \alpha$, $N_{\dot{\beta}}\dot{\psi} \sin \alpha$, $N_{\dot{\psi}}\dot{\psi} \sin \alpha$, $L_\beta \psi \cos \alpha$, $L_{\dot{\psi}}\dot{\psi} \cos \alpha$, and $L_{\dot{\beta}}\dot{\beta} \cos \alpha$, so that equation (3) becomes

$$L_t - L_\beta \psi \cos \alpha + N_\beta \psi \sin \alpha = -\left(L_{\dot{\psi}} - L_{\dot{\beta}}\right)\dot{\psi} \cos \alpha + \left(N_{\dot{\psi}} - N_{\dot{\beta}}\right)\dot{\psi} \sin \alpha \tag{4}$$

The motion when referred to the body axis is composed of both yaw and roll such that $\sin \psi_B/2 = \cos \alpha \sin \psi/2$ and $\sin -\phi_B/2 = \sin \alpha \sin \psi/2$; or for small angles encountered in the tests of this report, $\psi_B = \psi \cos \alpha$, $-\phi_B = \psi \sin \alpha$, $\dot{\psi}_B = \dot{\psi} \cos \alpha$, and $-\dot{\phi}_B = \dot{\psi} \sin \alpha$. Equation (3) then becomes

$$L_t - L_{\beta_B}\psi_B + L_{\dot{\phi}_B}\phi_B + \left(L_{\dot{\psi}_B} - L_{\dot{\beta}_B}\right)\dot{\beta}_B + L_{\dot{\phi}_B}\dot{\phi}_B = 0 \tag{5}$$

[redacted]

or

$$L_t - L_{\beta-B}(\psi \cos \alpha) + L_{\phi_B}(-\psi \sin \alpha) -$$

$$\left(L_{\dot{\psi}-B} - L_{\dot{\beta}-B}\right)\dot{\psi} \cos \alpha + L_{\dot{\phi}_B}\dot{\psi} \sin \alpha = 0 \qquad (6)$$

No attempt has been made in the presentation of the results to correct the data to either set of axes. For the angles of attack tested in this report the corrections are relatively small. To correct to the stability axis system, equation (4) should be used. At $\beta = 0^\circ$, it can be seen that, to correct the results to the stability axis system, information on $C_{n_r} - C_{n_{\dot{\beta}}}$ at angles of attack is needed and no experimental results are available for this airplane at supersonic speeds. To correct to the body axis system, equation (6) should be used. At $\beta = 0^\circ$, it can be seen that information on L_{ϕ_B} (i.e., C_{l_p}) is needed. An unpublished value of $C_{l_p} = -0.314$ for this airplane at $\alpha = 0^\circ$ and $M = 1.62$ has been measured in wind-tunnel tests. Assuming little change in C_{l_p} with angle of attack for the range tested, the $C_{l_r} - C_{l_{\dot{\beta}}}$ results presented in this investigation contain a $C_{l_p} \sin \alpha$ contribution with amounts to about -0.03 at an angle of attack of 8°.

Prior to the tests, the model was balanced about its body axis with lead weights glued in the hollow-nose section. This eliminated inertia forces being transmitted to the balance if the angular acceleration were other than zero. Also the selection of the pivot point at the center of gravity of the model further eliminated any inertia force being transmitted to the balance if any slight static unbalance about the body axis should still exist, and if the motion should be other than zero angular acceleration.

Calibration

The accuracy of the cam in producing the prescribed motion was checked prior to the tests by rotating it in precise 4.5° increments (using a milling machine dividing head) and reading the resultant model angle of yaw. The model angle of yaw was determined by using an optical setup with an 80-inch arm similar to the setup later used while actually conducting the static tests.

[redacted]

The lack of interaction of the roll balance with model lift and pitching moment was checked prior to the tests by using a Brown Recordax as the recording instrument. Calibrations of the strain-gage balance were also made throughout the test program using both the Brown Recordax and the camera technique since it was necessary to cut and resolder the strain-gage leads whenever the Mach number was changed and for some model changes.

A special setup was made to calibrate the instrument lag in the galvanometer elements of the oscillograph for various operating frequencies. Figure 7 illustrates the orientation of the apparatus for making this calibration. The roll balance was clamped rigidly in a vertical position. A yoke with a means for varying the moment arm of two lead weights was clamped to the balance. Also on the yoke was a small 1/16-inch-diameter mirror which reflected the light from a line source onto the film of the drum camera about 9 feet away. The strain-gage signal from the balance was fed through the Carrier-Amplifier into the oscillograph of the drum camera. With the drum camera revolving, the yoke-balance unit was plucked and a simultaneous dynamic record of the balance deflection and strain-gage signal was obtained on the film. The phase lag between these two traces on the film represented the instrument lag of the galvanometer elements of the oscillograph. Traces which determined this lag were obtained at various frequencies by varying the moment arm of the lead weights and thus changing the natural frequency of oscillation of the yoke-balance unit. Figure 8 shows the results of this calibration. Instrument lags of the order of 0.0007 second were measured which corresponded to a distance on the film of about 0.08 inch. The indicated accuracies shown in figure 8 were assessed by checking for symmetry each peak of the γ trace and of the moment trace.

Static Tests

The tests of this investigation were of two types: static and dynamic. The static tests furnished C_{l_β} data and were also used as a calibration in reducing the γ trace of a dynamic test. The technique of making a static test was as follows:

The model was clamped at a known angle of yaw indicated by the optical system with an 80-inch arm; the light source for this optical system was then extinguished and both shutters opened manually; with the shutters open, the drum of the camera was then manually rotated through a portion of a revolution, following which the shutters were closed. The model was then set at a new angle of yaw and the process repeated. The end product of a static test was a film record with a series of straight lines. Since the traces representing the yaw angle were at known values of the angle of yaw, the distance from the reference line that was measured on the film was used to compute the effective

radius from the model mirror to the film using the relation $\frac{\Delta h}{R} = \tan \psi$. A typical plot of the variation in R for various ψ or Δh values is shown in figure 9. The arrows at points A and B indicate the inaccuracy that would result from ±0.01-inch amplitude on the film. A curve such as figure 9 was used later in the reduction of data to obtain the values of ψ.

The angle of yaw variation was from about -10° to $+10^\circ$ in 2° increments. It was necessary to stop the tunnel and readjust the oblique mirror of the optical system producing the ψ trace on the film when the angle of attack of the model was changed.

Tests were conducted for angles of attack from 0° to about 8° for the complete configuration at Mach numbers of 1.62, 1.94, and 2.41. Also component tests of the body-wing configuration, and of the body-tail configuration were conducted for the same angle-of-attack and angle-of-yaw range at Mach numbers 1.62 and 2.41.

The Reynolds numbers of the tests (based on the wing mean aerodynamic chord) were 0.454×10^6 at $M = 1.62$, 0.524×10^6 at $M = 1.94$, and 0.624×10^6 at $M = 2.41$. Transition strips, made of finely ground salt, were glued near the leading edges of all wing and tail surfaces and near the nose of the body in order to simulate more closely the higher Reynolds number boundary-layer conditions such as might be experienced in the flight of the prototype. Figure 1 illustrates the location of these strips.

Dynamic Tests

Immediately following each static test, without stopping the tunnel, the dynamic tests were conducted at two values of model oscillating frequency. These frequencies were about 200 and about 320 cycles per minute. The latter frequency corresponds to a yawing velocity of the full-scale airplane of about 0.1 radian per second. The technique for conducting a dynamic test was as follows:

After checking the adjustment of the timing light, the model oscillating frequency was adjusted and held constant; the drum speed of the camera was adjusted and held constant; then the manual switch which activated the automatic shutters was triggered.

The check of the adjustment of the frequency of the timing light was made prior to each dynamic test by feeding the signal light from the oscillator into the Stroboconn. After adjusting the frequency to the desired value (200 cylces per second for most of the tests), the signal from the oscillator was switched to one of the galvanometer elements of

the oscillograph and furnished an accurate timing record on the film. The light from one of the reference mirrors was superposed on the timing light trace in order to define conveniently each cycle of the trace.

A sample portion of about 1 cycle of a film record is shown greatly reduced in figure 10 and a sketch of a similar record with the essential portions labeled is shown in figure 11. Each film record actually contained about 5 cycles. Only that portion of each cycle which was at constant angular velocity (the straight-line portion) was used in the reduction of the data. The illustrated wiggle in the ψ trace of the particular record shown in figure 10 could be ignored since it occurred during a portion of the cycle not used in the reduction of the data.

DATA REDUCTION

The reduction of the data of a static test consisted simply of measuring the distance between the reference line and both the moment trace and the angular position trace, multiplying the moment measurement by the appropriate constant and plotting against the known values of angular position. The angular position measurements of the film were used later as a calibration of the ψ trace of a dynamic test. The results of the static tests are shown in figures 12 to 15 and the dynamic data are shown in figures 16 to 22.

Prior to the mechanical reduction of a film record of a dynamic test an accurate knowledge of the model oscillating frequency was obtained using the linear portion of the ψ trace to find the variation in ψ within a given time; the time for this variation was obtained from the timing light trace. Also prior to the mechanical reduction of the data, a faired line was inked on the film to replace the moment trace in order to make the reading of the film easier if hash existed in the moment trace.

The mechanical film reading process then furnished a rapid means of measuring and recording the distance from the reference line to the ψ trace and to the moment trace. These readings were taken for each integer cycle of the timing light trace corresponding to a known time between each reading of about 0.005 second for most of the tests. The measurements were made throughout every data portion on each film record, furnishing two sets of readings for each cycle of the model. Multiplying each moment reading by a constant determined from the balance calibration and from q, S, and b, gave C_l directly. Dividing each ψ reading by the appropriate value of R (obtained from a curve such as figure 9) determined the corresponding value of $\tan \psi$, from which ψ was obtained.

[redacted]

The galvanometer lag was accounted for during the film reading process by reading the moment trace an instant of time later on the film than the reading for the ψ trace. The instrument lag corresponding to the model oscillating frequency was determined prior to the film reading process by referring to the calibration curve of figure 8 and this was converted into a known distance on the film by which the moment reading should lag the ψ reading. This distance was of the order of 0.08 inch on the film for the high frequency tests.

In order to illustrate the method of the extraction of the derivative $C_{l_r} - C_{l_{\dot{\beta}}}$ from the data, the solid-line traces of figure 11 present a sketch of how the data reduced in the preceding manner might appear if plotted against time. The moment trace will either lag or lead the force trace (by a distance c or d of figure 11) depending on the direction of the force associated with the derivatives $C_{l_r} - C_{l_{\dot{\beta}}}$. In accordance with equation (3) it can be seen that at $\psi = 0$ the distances a and b of figure 11 represent the moment associated with the derivative $C_{l_r} - C_{l_{\dot{\beta}}}$. The data, although applicable at all the ψ values within the linear range, can be more simply extracted at $\psi = 0$.

The line AB of figure 11 represents the location of zero moment and zero ψ on their respective traces. It can be seen that the misplacement of this line would result in unequal lag or lead and unequal values of the cross derivative during a $+\dot{\psi}$ section of the trace as compared with a $-\dot{\psi}$ section. This property afforded a convenient means of obtaining the zero moment reference when the zero ψ reference was known, and was used in the reduction of the data. The zero position of the ψ trace was obtained from the static test which immediately preceded the dynamic tests.

PRECISION

Motion

The previously mentioned check of the accuracy of the cam in producing the prescribed motion indicated that the cam would produce a linear angle-of-yaw variation of the model to within $\pm 0.03^\circ$ if rotated at constant speed. The linearity of the $\dot{\psi}$ trace on the film record was the only means for assessing the constancy of the cam rotational speed and should be used as the true standard as to the accuracy of the motion. On the full-scale film records it was possible to detect a slight bow in the ψ trace which would amount to about 1.5-percent change in slope in traversing from about -7° to $+7^\circ$ yaw angle. It is believed that this error is negligible, since the data are concerned only

[redacted]

with changes in ψ and corresponding changes in C_l such as would occur over smaller periods of time than the time for the model to traverse the complete linear range of -7° to $+7^\circ$.

Balance and Recording Apparatus

The repeated calibrations throughout the tests using both a Brown Recordax and the camera technique for indicating the strain-gage readings, disclosed that the inaccuracy and insensitivity associated with the camera technique masked the actual error associated with the strain-gage balance itself. Thus, the accuracy of any point measured during a test depended on the accuracy of the camera technique. Inaccuracies in the camera technique would result from film distortion during developing and drying, a wrinkle in the film due to faulty loading of the camera, and the inability to read a poor film record with accuracy. For the static tests this latter cause was significant and resulted in greater inaccuracy in the static data than is believed to exist in the dynamic data. The poorer film records of the static tests were associated with the fact that when the drum was rotated manually a portion of a revolution, much wider light traces resulted. Also, centrifugal force was not helping to hold the film flat against the drum.

Estimated Resulting Accuracy of the Cross Derivative

An overall estimate of the final resulting accuracy of the $C_{l_r} - C_{l_{\dot{\beta}}}$ values is very difficult to make. An estimate of the accuracy of any individual point of a C_l against ψ curve for a dynamic test would be misleading since the value of a cross derivative depended on a faired curve through many points. However, as a guide in estimating the accuracy of the cross derivative the following probable errors pertaining to an individual point are presented. An increment of ±0.01 inch on the film represents an accuracy that would apply to the majority of the test points. This would correspond to a ΔC_l of ±0.00022 at $M = 1.62$. The measure of C_l at $\psi = 0$ furnished the parameter $\left(C_{l_{\dot{\psi}}} - C_{l_{\dot{\beta}}}'\right)\dot{\psi}$. Thus an error in the moment trace of ±0.01 inch for a typical high frequency test at about 5.1 radians per second would contribute to an error in $C_{l_{\dot{\psi}}} - C_{l_{\dot{\beta}}}'$ of ±0.000041 at $M = 1.62$. Since

$$C_{l_r} - C_{l_{\dot{\beta}}} = 8{,}690\left(C_{l_{\dot{\psi}}} - C_{l_{\dot{\beta}}}'\right)$$

[redacted]

at $M = 1.62$, this would correspond to an error in $C_{l_r} - C_{l_{\dot{\beta}}}$ of ±0.38. The inaccuracy in $\dot{\psi}$ which appeared to be as high as 6 percent between the various cycles of any one family of points would revise the error in $C_{l_r} - C_{l_{\dot{\beta}}}$ upward to about ±0.41. For a typical low-frequency test, the corresponding error in $C_{l_r} - C_{l_{\dot{\beta}}}$ would be about ±0.58. As mentioned, this analysis of the accuracy based on individual point measurements is misleading. Another method used to assess the accuracy was to fair limiting curves through the data of figures 16 to 22 with the maximum spread that could conceivably be faired corresponding to the scatter of the test points. Combining these limiting curves with the maximum errors in the determination of the frequency (combined in the worse manner) determined a conservative estimate of the accuracy. The shaded area of figure 23 illustrates the maximum possible error determined in this manner. This method is believed a better indication of the accuracy than the analysis based on individual point measurements, although it also is possibly too conservative.

RESULTS AND DISCUSSION

Static Tests

As mentioned previously, the data from the static tests were subject to greater inaccuracies than the data of the dynamic tests. The static data of C_l against β are presented in figures 12 to 14, and the variation of C_{l_β} (per degree) with angle of attack is shown in figure 15 for the various configurations. It should be remembered that at angles of attack other than 0°, the data as presented are the rolling moment measured about the body axis due to a sideslip as measured in the stability axis system. Included in reference 8 are similar data for this airplane at Mach numbers 1.61 and 2.01. The data, where comparisons are appropriate, compare favorably if it is remembered that the airplane of reference 8 had a slightly smaller vertical tail. Comparison of the data at Mach number 1.62 for this investigation with that at Mach number 1.61 of reference 8 shows that the C_{l_β} values are almost identical for the complete airplane at zero angle of attack. The body-tail results (complete vertical and horizontal tail) of the airplane of this investigation are more negative than the C_{l_β} results of reference 8 for the vertical tail alone. Both investigations indicate the body-wing contribution to C_{l_β} is practically zero at zero angle of attack.

The data of this investigation show a decided effect of angle of attack on C_{l_β}, due to the wing contribution to this derivative, especially

at Mach number 2.41. It is interesting to note that, based on the data at $M = 1.62$ and $M = 2.41$, there is a decrease in the contribution of the body-tail to C_{l_β} with increasing Mach number and an increase in the contribution of the body-wing with increasing Mach number. For the complete configuration at zero angle of attack, no variation in C_{l_β} with Mach number was evident for all three test Mach numbers. The effect of angle of attack on C_{l_β} appears less at Mach number 1.94 than for either the higher or lower Mach numbers.

Dynamic Tests

Figures 16 to 22 present the dynamic variation of rolling-moment coefficient with angle of yaw. High-frequency and low-frequency data are plotted for the same configuration on offset axes. Any one set of symbols on a curve represents the values along one data portion of a cycle at known constant time increments. The flagged symbols are taken from positive slopes ($+\dot{\psi}$ motion) and the unflagged symbols from negative slopes ($-\dot{\psi}$ motion). With a phase lag between the moment trace and the angular position trace, the vertical distance between the two families of data (flagged or unflagged) will represent twice the rolling moment due to the motion. Figures 16 to 22 indicate that most of the curves of the two families of data are reasonably parallel and show little effect of β on the magnitude of the cross derivative so attention can be confined to the results at $\psi = 0$ for greater simplicity. Equation (3) illustrates that at $\psi = 0$ the strain gage reads the cross-derivative parameter $-\left(L_{\dot{\psi}} - L_{\dot{\beta}}\right)\dot{\psi}$ directly. The coefficient $C_{l_r} - C_{l_{\dot{\beta}}}$ associated with this moment is obtained by dividing half the distance between the two families of data at $\psi = 0$ by $\dot{\psi}$ and multiplying by $2V/b$.

Figures 23, 24, and 25 present the variation of $C_{l_r} - C_{l_{\dot{\beta}}}$ with angle of attack and frequency for the configurations tested. The surprising result that the wing has a large negative contribution to $C_{l_r} - C_{l_{\dot{\beta}}}$ is illustrated in figures 23(c) and 25(c). This means that yawing and sideslipping to the right produces a negative rolling moment and the moment associated with this motion would contribute to a divergent motion of the airplane. Reference 12 shows that such a motion is encountered inadvertently during flight tests of the full-scale airplane at low angles of attack. At higher angles of attack the airplane is more stable. It should be emphasized, however, that the derivative $C_{l_r} - C_{l_{\dot{\beta}}}$ is not the chief cause of the divergent motion experienced by the full-scale airplane but that (as pointed out in ref. 12) the inclination of the principal axis relative to the flight path has a pronounced influence on

the motion of the airplane. The aforementioned negative values of $C_{l_r} - C_{l_{\dot{\beta}}}$ occur in spite of the fact that the static derivative C_{l_β} due to the wing is slightly negative; that is, positive yaw produces positive roll. The inadequacy of the approximation associated with the method of estimating dynamic derivatives using experimental values of the sideslip derivatives such as is considered in reference 7, is clearly demonstrated, since for this particular configuration such a procedure would lead to a value of C_{l_r} of only about 0.1. This value is considerably different in sign and magnitude from $C_{l_r} - C_{l_{\dot{\beta}}}$ values measured in the investigation of this report.

The cause of the negative values of $C_{l_r} - C_{l_{\dot{\beta}}}$ is not obvious since the wing had 3° incidence and 3° negative dihedral. Reference 13 indicates that a sweptback wing can have negative C_{l_r} values, but a theoretical prediction of C_{l_r} for the wing or wing body of the airplane of this investigation has not been attempted.

Because the complete configuration data and the body-wing data at Mach number 2.41 were tested early in the program before testing experience indicated some possible improvements in the apparatus, there was more hash in the moment trace of these tests and the results are believed to be less accurate than for the remaining tests. (The improvement in the apparatus consisted of replacing the spring which held the rocker arm to the cam with a 6-foot length of elastic shock cord.) Figure 23, which represents the results at Mach number 1.62, shows that for the complete configuration the large negative $C_{l_r} - C_{l_{\dot{\beta}}}$ values of the wing are predominant as compared with the positive $C_{l_r} - C_{l_{\dot{\beta}}}$ values of the body tail.

At Mach numbers 1.62 and 1.94 the effects of frequency on $C_{l_r} - C_{l_{\dot{\beta}}}$ are small and are believed to probably be within the accuracy of the data. Because of the greater inaccuracy of the data at Mach number 2.41, the larger effect of frequency that is shown is believed to be questionable. However, the order of magnitude of the derivative and its variation through the angle-of-attack range is evident from the results presented in figures 23, 24, and 25 and should be considered reliable.

Significance of Results

Because of the large discrepancy between the measured value of the derivative and previous crude estimates (for example as used in ref. 7)

an attempt was made to assess its effect on the final motion of the airplane by calculations of the period and damping. The results of these calculations are presented merely as a guide by which to regard the measurements of the cross derivative of this investigation in the proper perspective. The strong interaction of the derivatives in the equations of motion prohibits generalizing on the effects of any one derivative, since for a different combination of values of the other derivatives, entirely different results might be obtained.

The calculations of the period and damping were made for two different angle-of-attack conditions at a Mach number of 1.6 and for an altitude of 50,000 feet. All the other derivatives being the same, the effect of various values of C_{l_r} and $C_{l_{\dot{\beta}}}$ on the period and damping of the oscillating mode and on the damping of the spiral and the roll mode can be compared. The values of the mass, geometry, and inertia characteristics were the same as used in reference 10 and were $W/S = 60$, $S = 175$ square feet, $b = 25$ feet, $\epsilon = 3.7^\circ$, $I_{x_o} = 3{,}150$ slug-feet^2, $k_{x_o} = 3.12$ feet, and $k_{z_o} = 9.86$ feet. The sideslip derivatives used in the calculations were obtained from the experimental measurements of reference 8 at $M = 1.61$. The values of these sideslip derivatives were $C_{l_\beta} = -0.07445$, $C_{n_\beta} = 0.0916$, and $C_{Y_\beta} = -0.7215$. A value of C_{l_p} of -0.314 was used, based on unpublished Langley 9-inch supersonic tunnel tests. The derivatives C_{Y_p}, C_{Y_r}, and $C_{Y_{\dot{\beta}}}$ were assumed to be zero in accordance with the calculations of reference 10 which indicated that sizable changes in the values of these derivatives have a negligible effect on the damping. The values of C_{n_p} and C_{n_r} which were used were based on the crude approximation indicated in reference 7 and $C_{n_{\dot{\beta}}}$ was assumed zero in the absence of a better method to estimate readily these derivatives. The results of the calculations are presented in the following table:

[redacted]

α	$C_{l_r} - C_{l_{\dot{\beta}}}$	Assumed proportion of C_{l_r} to $C_{l_{\dot{\beta}}}$	Spiral mode $T_{1/2-1}$	Roll mode $T_{1/2-2}$	Lateral oscillatory mode	
					$T_{1/2-3}$	P
0.5	0.0747	$C_{l_{\dot{\beta}}} = 0$	88.5	0.39	-37.5	3.2
.5	-.52	$C_{l_{\dot{\beta}}} = 0$	21.3	.39	19.7	3.2
.5	-.52	$C_{l_r}/C_{l_{\dot{\beta}}} = 4$	17.2	.39	22.8	3.2
.5	-.52	$C_{l_r}/C_{l_{\dot{\beta}}} = 2$	12.7	.39	22.8	3.2
4.0	.0747	$C_{l_{\dot{\beta}}} = 0$	27.6	.49	4.2	2.7
4.0	-.78	$C_{l_{\dot{\beta}}} = 0$	4.6	.53	4.0	2.7
4.0	-.78	$C_{l_r}/C_{l_{\dot{\beta}}} = 4$	3.5	.55	4.3	2.7
4.0	-.78	$C_{l_r}/C_{l_{\dot{\beta}}} = 2$	2.3	.57	5.6	2.7

For the low angle-of-attack condition, there is no effect of the cross derivative on the damping of the roll mode and a negligible affect on the period of the oscillatory mode. The damping of the spiral mode changes with the proportion of C_{l_r} to $C_{l_{\dot{\beta}}}$, but is affected greater by the change from the previous estimated value $\left(C_{l_r} = 0.0747, \quad C_{l_{\dot{\beta}}} = 0\right)$ to the experimental value of $C_{l_r} - C_{l_{\dot{\beta}}}$ (-0.52). Even this change might not be noticeable to a pilot, however. The damping of the oscillatory mode is affected slightly by different proportions of C_{l_r} to $C_{l_{\dot{\beta}}}$ but its largest change also results from the use of the experimental value as compared to the previous estimated value. At this flight condition the motion is slightly damped if the experimental value is used and slightly unstable (the negative value denotes time to double amplitude) if the previous estimate is used. Both conditions are so near neutrally stable, however, that even the difference between the experimental and previously estimated values does not illustrate decided differences in the dynamic performance of the airplane. The results of the calculations at the higher angle-of-attack condition illustrate the greater stability of the airplane at higher angle of attack but, with the exception of the spiral mode, the value of the cross derivative is shown to be unimportant for the condition investigated.

Although the preceding analysis shows the final resulting motion of the airplane to be relatively insensitive to changes in the derivative $C_{l_r} - C_{l_{\dot{\beta}}}$ for the particular condition investigated, this might not occur

[redacted]

for other flight conditions, for example, a different Mach number, a different altitude, or an angle of climb other than 0°. It should also be remembered that establishing the magnitude of this derivative has a value in interpreting flight results. For example, in using the rotating vector method to obtain the derivatives from a given flight history of an airplane as was done in reference 6, the problem reduces to a point where three derivatives are unknown but the directions are known, and it is necessary to estimate one of the derivatives in order to close the polygon. Usually it is the derivative $C_{l_r} - C_{l_{\dot{\beta}}}$ that is estimated and the other two, C_{l_p} and C_{l_β}, are determined accordingly. This is because $C_{l_r} - C_{l_{\dot{\beta}}}$ is usually the smallest. The results of this investigation indicate that a great deal of care should be used in such a procedure since the derivative $C_{l_r} - C_{l_{\dot{\beta}}}$ can be sizeable in magnitude and of opposite sign than considerations based on the contribution of the vertical tail by itself would indicate. For the lack of any tests or adequate theory the wing contribution to this derivative was often neglected and as is shown by the investigation of this report would result in a completely unrealistic value of $C_{l_r} - C_{l_{\dot{\beta}}}$.

CONCLUSIONS

A technique is described for measuring $C_{l_r} - C_{l_\beta}$ (rolling moment due to yawing velocity and to acceleration in sideslip) of an airplane and its components at supersonic speeds. The sideslip derivative C_{l_β} is obtained as a byproduct when using this technique. The application of the technique to the Douglas D-558-II complete airplane configuration at Mach numbers 1.62, 1.94, and 2.41 and to the component tests of the body-wing and the body-tail at Mach numbers 1.62 and 2.41, all of which were tested through an angle-of-attack range from 0° to 8°, yielded the following conclusions:

1. The wing-body at zero angle of attack had a negligible contribution to C_{l_β} of the complete airplane, but its contribution increased with angle of attack and produced a variation in C_{l_β} of the complete airplane that became increasingly negative with increasing angle of attack at Mach numbers 1.62 and 2.41. The body-tail had negligible variation in C_{l_β} with angle of attack. The tests of the complete configuration at Mach number 1.94 showed less variation in C_{l_β} with angle of attack than the complete-configuration data at the other Mach numbers.

2. The contribution of the body-tail to $C_{l_r} - C_{l_{\dot{\beta}}}$ was in the direction expected although larger in magnitude. However, the contribution of the body-wing to $C_{l_r} - C_{l_{\dot{\beta}}}$ was predominant in its effect on the resulting $C_{l_r} - C_{l_{\dot{\beta}}}$ of the complete configuration and was negative. Whether this was due to the wing's negative dihedral or to its sweepback was not established, but the moment associated with this derivative would contribute to a divergent motion of the airplane. (Yawing to the right would cause a negative rolling moment.) This negative value of $C_{l_r} - C_{l_{\dot{\beta}}}$ occurred even though C_{l_β} was negative. (A positive yaw angle would cause a positive rolling moment.)

3. An analysis of the effect of the large discrepancy between the previously estimated value of $C_{l_r} - C_{l_{\dot{\beta}}}$ compared to the measured value of this report, involving period and damping calculations of the full-scale airplane, disclosed that, at a moderate angle of attack (4°), where the lateral oscillatory motion was stable, the order of magnitude of this derivative had a negligible effect on the motion of the airplane for the particular condition and combination of derivatives investigated. In the low angle-of-attack condition (0.5°), the use of the previously estimated value resulted in a slightly unstable oscillation; whereas the use of the measured value resulted in a slightly damped oscillation. These calculations cannot be considered as a conclusive indication of the degree of insensibility of the final motion of the airplane to the magnitude of this derivative due to the inadequate number of flight conditions investigated. However, establishing the magnitude of this derivative and showing the possibility of large negative contributions due to the wing body indicates the need for caution in estimating this derivative when extracting stability derivatives from flight motion studies.

Langley Aeronautical Laboratory,
National Advisory Committee for Aeronautics,
Langley Field, Va., August 5, 1955.

[redacted]

REFERENCES

1. Bird, John D., Fisher, Lewis R., and Hubbard, Sadie M.: Some Effects of Frequency on the Contribution of a Vertical Tail to the Free Aerodynamic Damping of a Model Oscillating in Yaw. NACA Rep. 1130, 1953. (Supersedes NACA TN 2657.)

2. Fisher, Lewis R., and Wolhart, Walter D.: Some Effects of Amplitude and Frequency on the Aerodynamic Damping of a Model Oscillating Continuously in Yaw. NACA TN 2766, 1952.

3. Fisher, Lewis R.: Some Effects of Aspect Ratio and Tail Length on the Contribution of a Vertical Tail to Unsteady Lateral Damping and Directional Stability of a Model Oscillating Continuously in Yaw. NACA TN 3121, 1954.

4. Bird, John D., and Jaquet, Byron M.: A Study of the Use of Experimental Stability Derivatives in the Calculation of the Lateral Disturbed Motions of a Swept-Wing Airplane and Comparison With Flight Results. NACA Rep. 1031, 1951. (Supersedes NACA TN 2013.)

5. Lessing, Henry C., Fryer, Thomas B., and Mead, Merrill H.: A System for Measuring the Dynamic Lateral Stability Derivatives in High-Speed Wind Tunnels. NACA TN 3348, 1954.

6. Mitchell, Jesse L., and Peck, Robert F.: Investigation of the Lateral Stability Characteristics of the Douglas X-3 Configuration at Mach Numbers From 0.6 to 1.1 by Means of Rocket-Propelled Model. NACA RM L54L20, 1955.

7. Campbell, John P., and McKinney, Marion O.: Summary of Methods for Calculating Dynamic Lateral Stability and Response and for Estimating Lateral Stability Derivatives. NACA Rep. 1098, 1952. (Supersedes NACA TN 2409.)

8. Grant, Frederick C., and Robinson, Ross B.: Static Lateral Stability Characteristics of a 1/16-Scale Model of the Douglas D-558-II Research Airplane at Mach Numbers of 1.61 and 2.01. NACA RM L53I29a, 1953.

9. Grigsby, Carl E.: An Investigation of the Effects of Jet Exhaust and Reynolds Number Upon the Flow Over the Vertical Stabilizer and Rudder of the Douglas D-558-II Research Airplane at Mach Numbers of 1.62, 1.93, and 2.41. NACA RM L54E03, 1954.

10. Queijo, M. J., and Goodman, Alex: Calculations of the Dynamic Lateral Stability Characteristics of the Douglas D-558-II Airplane in High-Speed Flight for Various Wing Loadings and Altitudes. NACA RM L50H16a, 1950.

[redacted]

11. Campbell, John P., and Woodling, Caroll H.: Calculated Effects of the Lateral Acceleration Derivatives on the Dynamic Lateral Stability of a Delta-Wing Airplane. NACA RM L54K26, 1955.

12. Ankenbruck, Herman O., and Wolowicz, Chester H.: Lateral Motions Encountered With the Douglas D-558-II All-Rocket Research Airplane During Exploratory Flights to a Mach Number of 2.0. NACA RM H54I27, 1954.

13. Goodman, Theodore R.: Dynamic Derivatives in Yaw and Sideslip of Thin Wings at Supersonic Speeds. Preprint No. 524, S.M.F. Fund Paper, Inst. Aero. Sci., Jan. 1955.

[redacted]

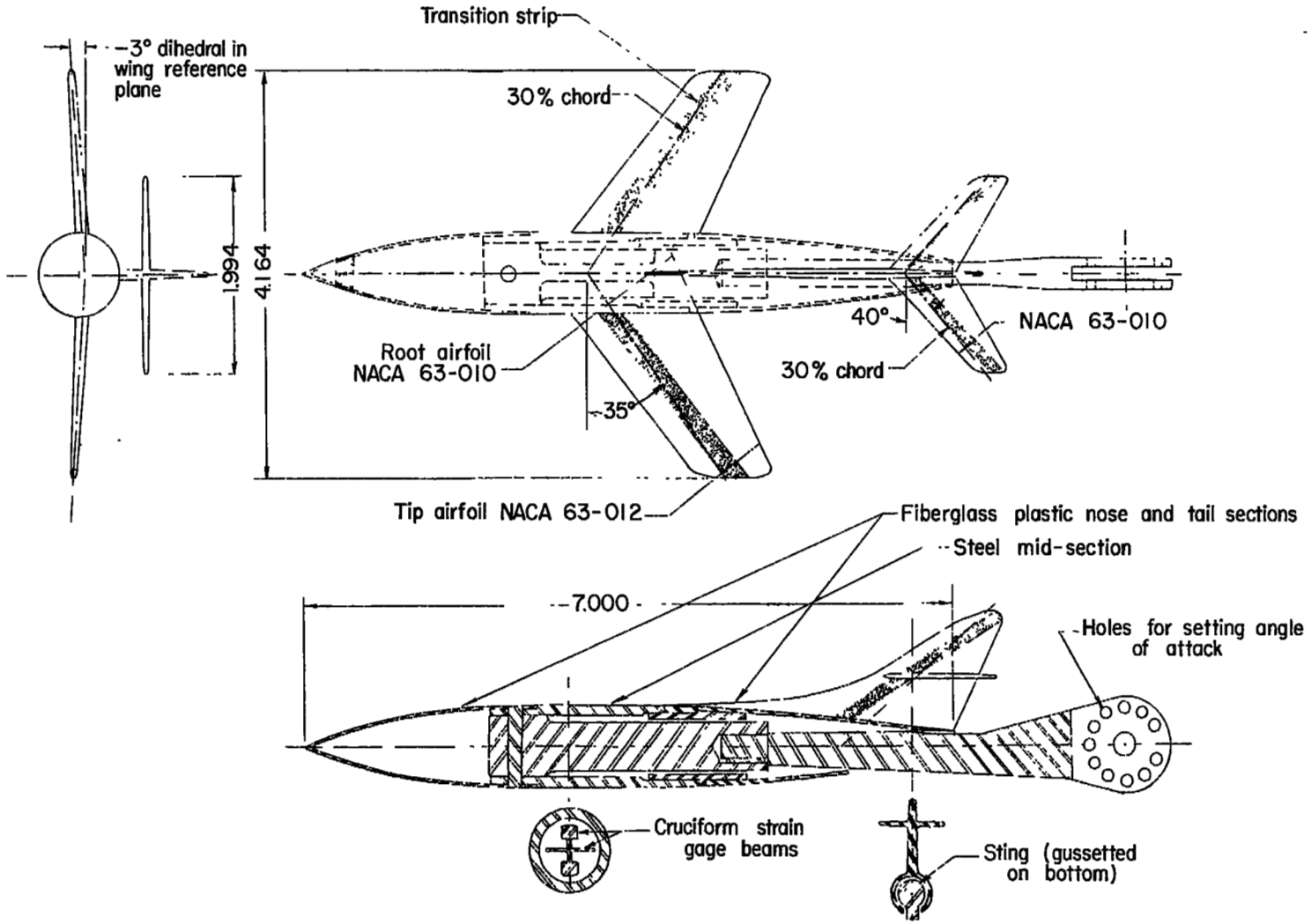

Figure 1.- Sketch of Douglas D-558-II model showing rolling-moment balance. (All dimensions are in inches.)

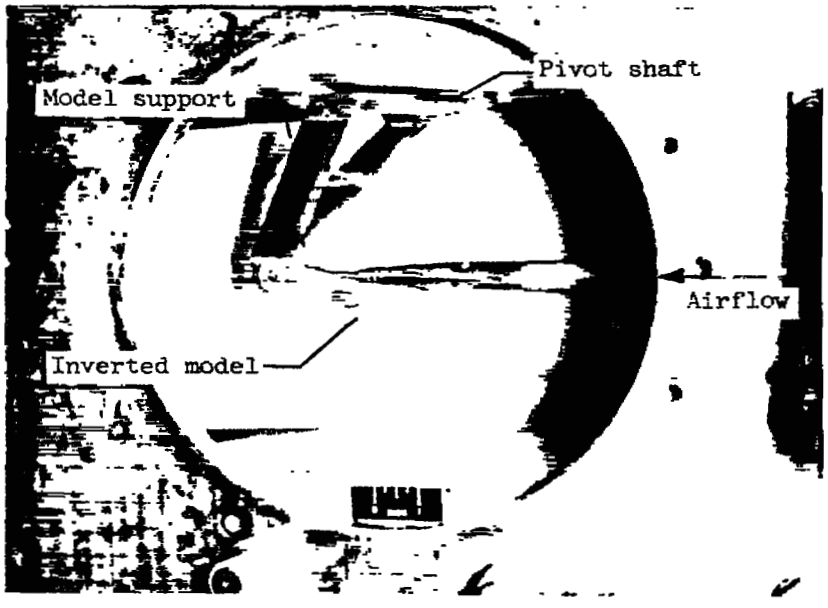

L-88012.1

Figure 2.- Photograph illustrating method of model support in the tunnel.

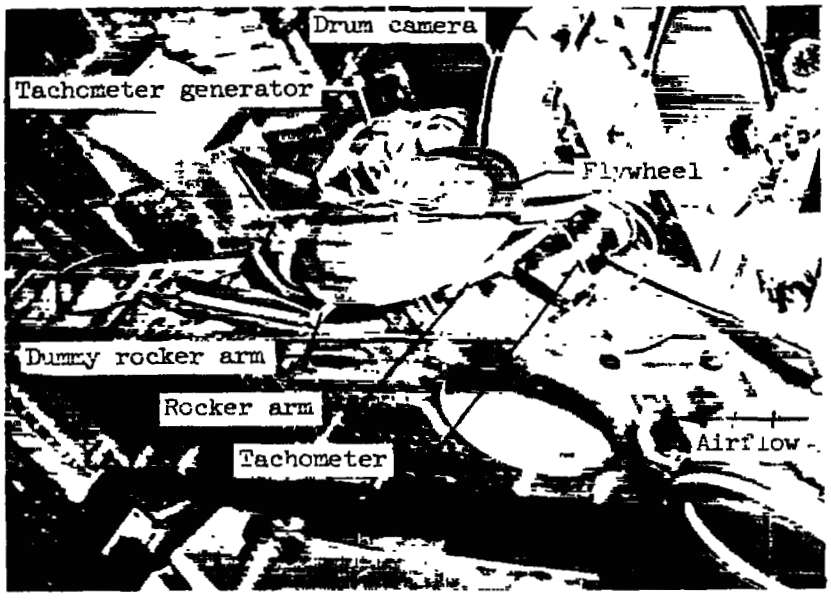

L-88013.1

Figure 3.- Photograph of model oscillating apparatus. (Viewed from above the tunnel looking downstream.)

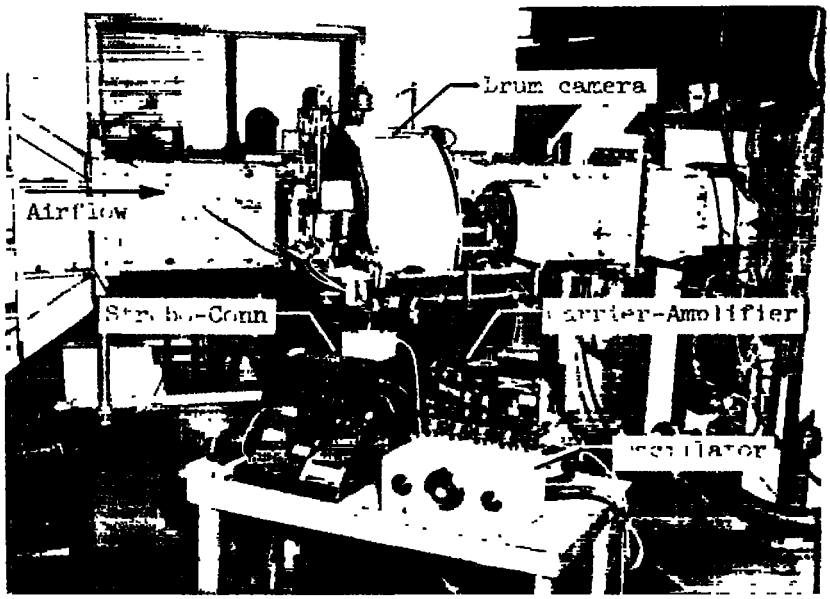

L-88016.1

Figure 4.- General view of drum camera mounted on side of tunnel with auxiliary equipment in foreground.

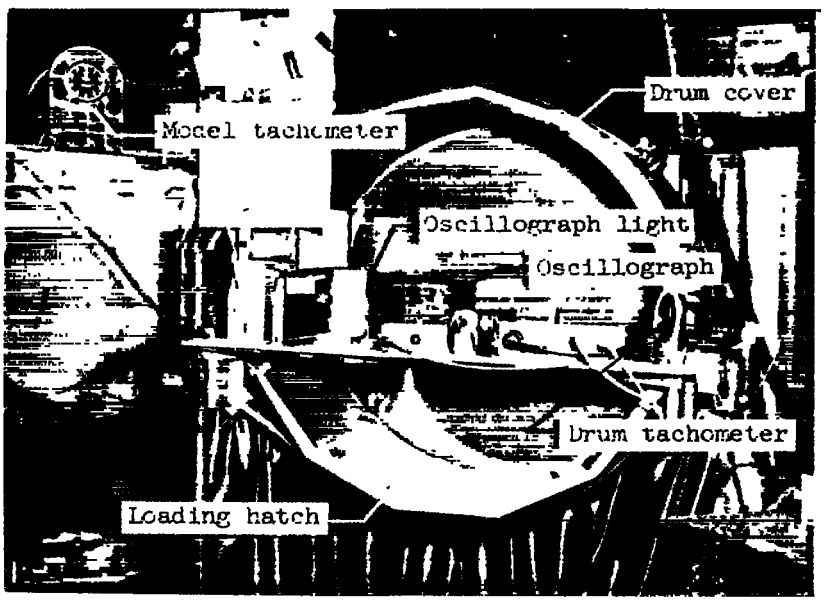

L-88014.1

Figure 5.- Close-up view of drum camera and oscillograph apparatus.

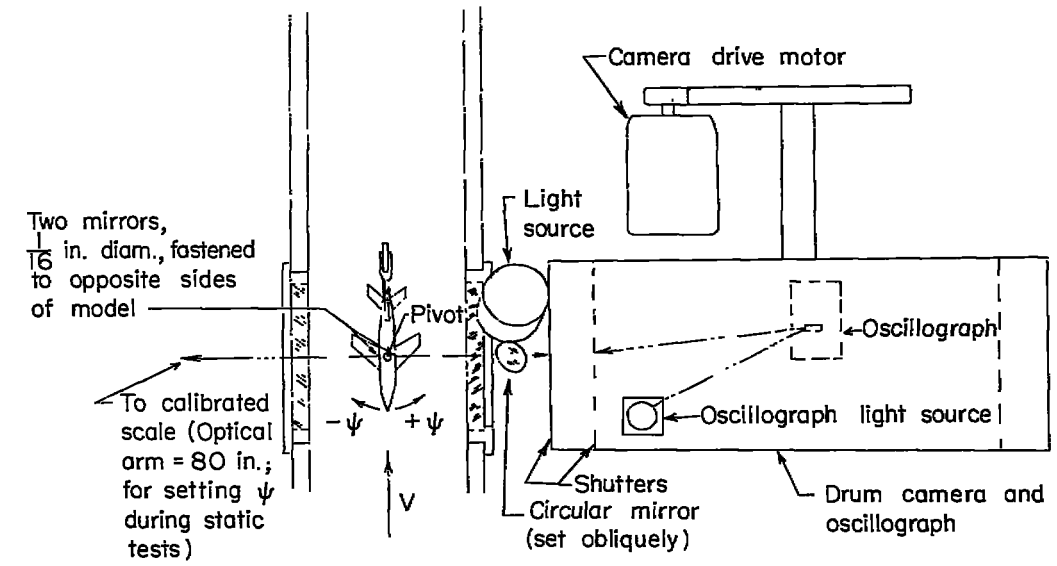

(a) Top view.

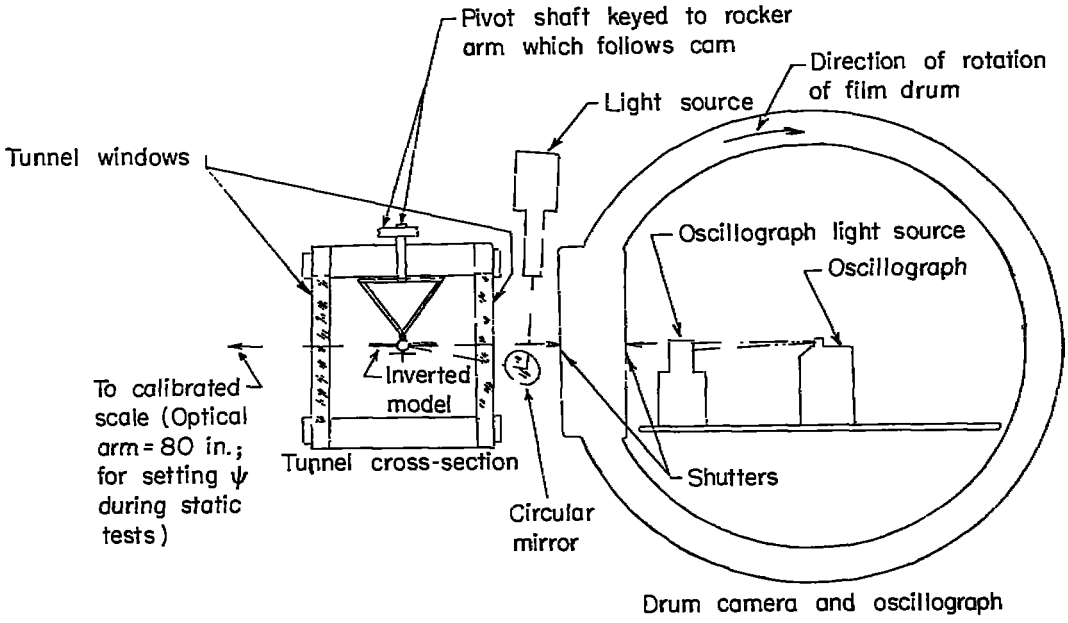

(b) Front view (looking downstream).

Figure 6.- Sketch of orientation of model, tunnel, drum camera and the paths of the various light beams used to record data and position of the model.

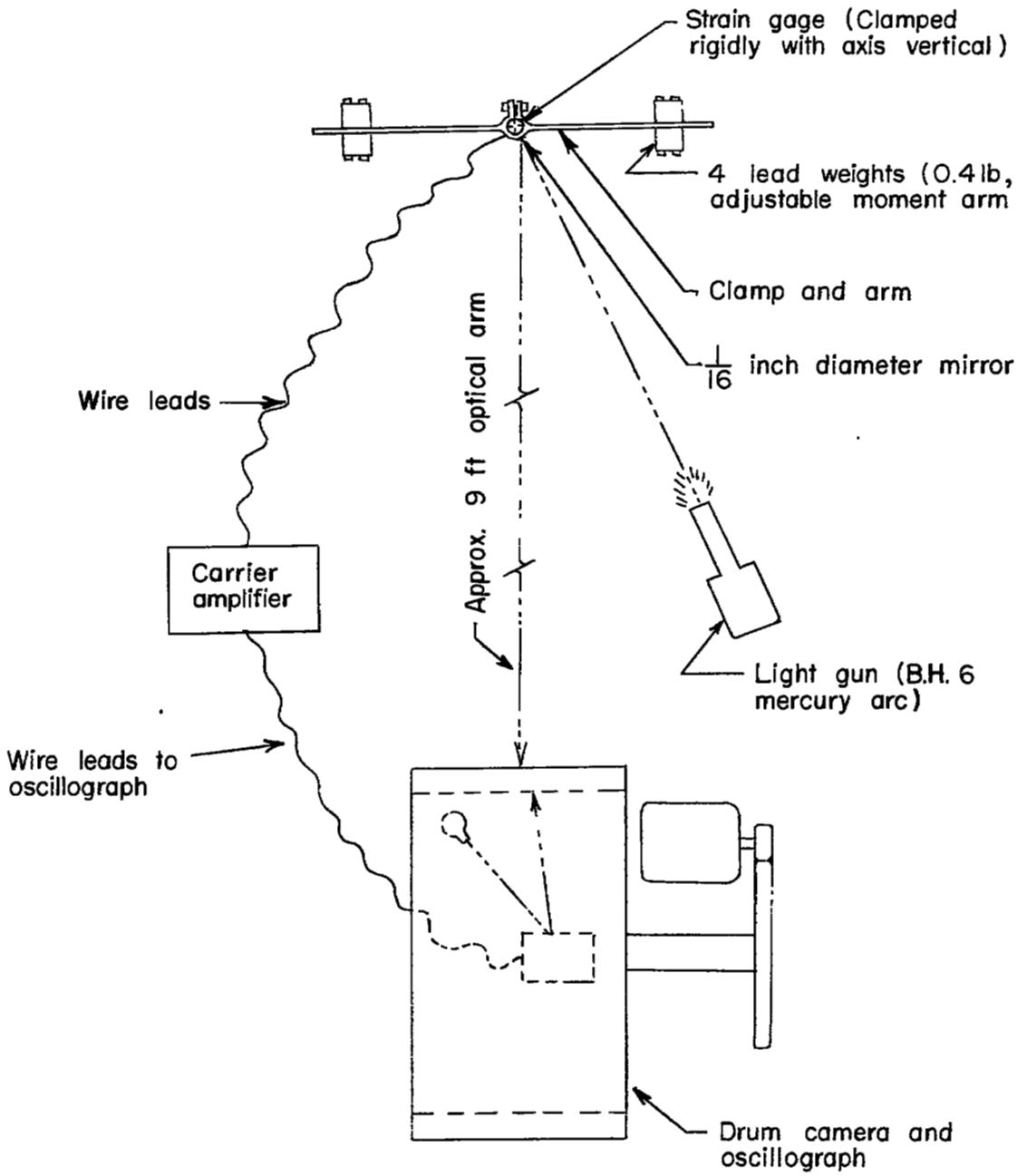

Figure 7.- Sketch of orientation of apparatus used in calibrating the instrument lag of the galvenometer elements of the oscillograph.

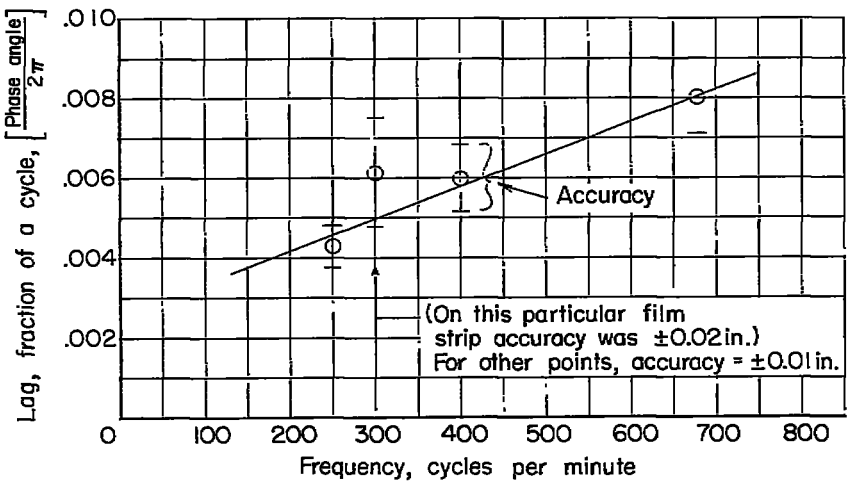

Figure 8.- Instrument lag of a galvenometer element of the oscillograph as a function of its operating frequency.

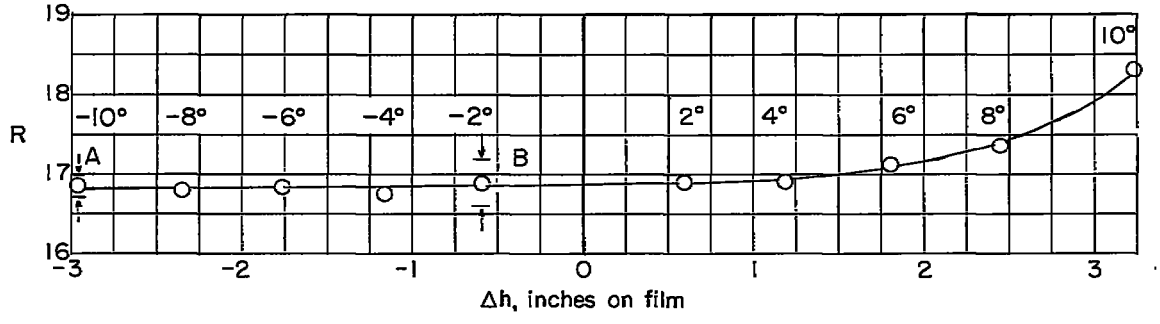

Figure 9.- A typical curve of the variation in R, the effective distance from the model mirror to the film as a function of the indicated amplitude on the film of the ψ trace.

[redacted]

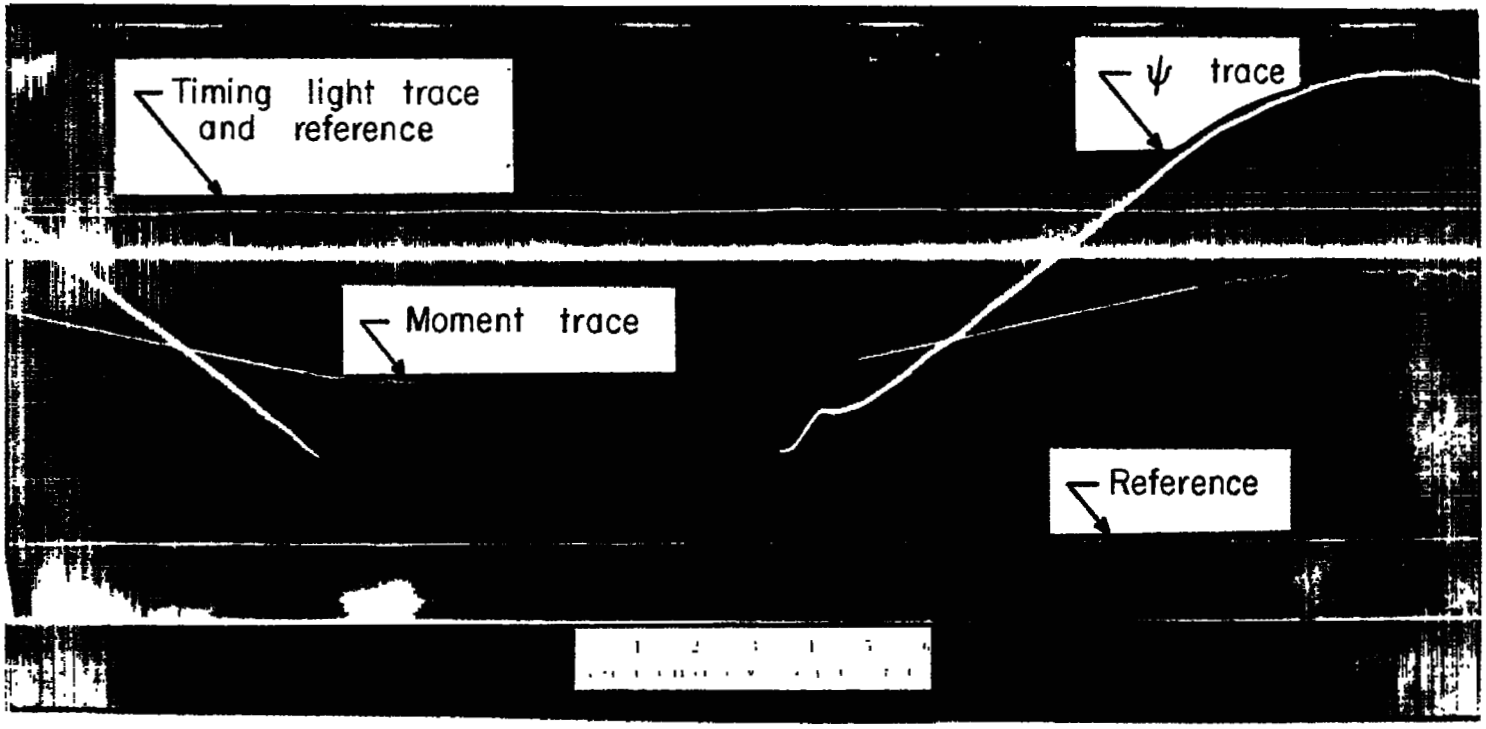

L-89386

Figure 10.- Photograph of a portion of a typical film record.

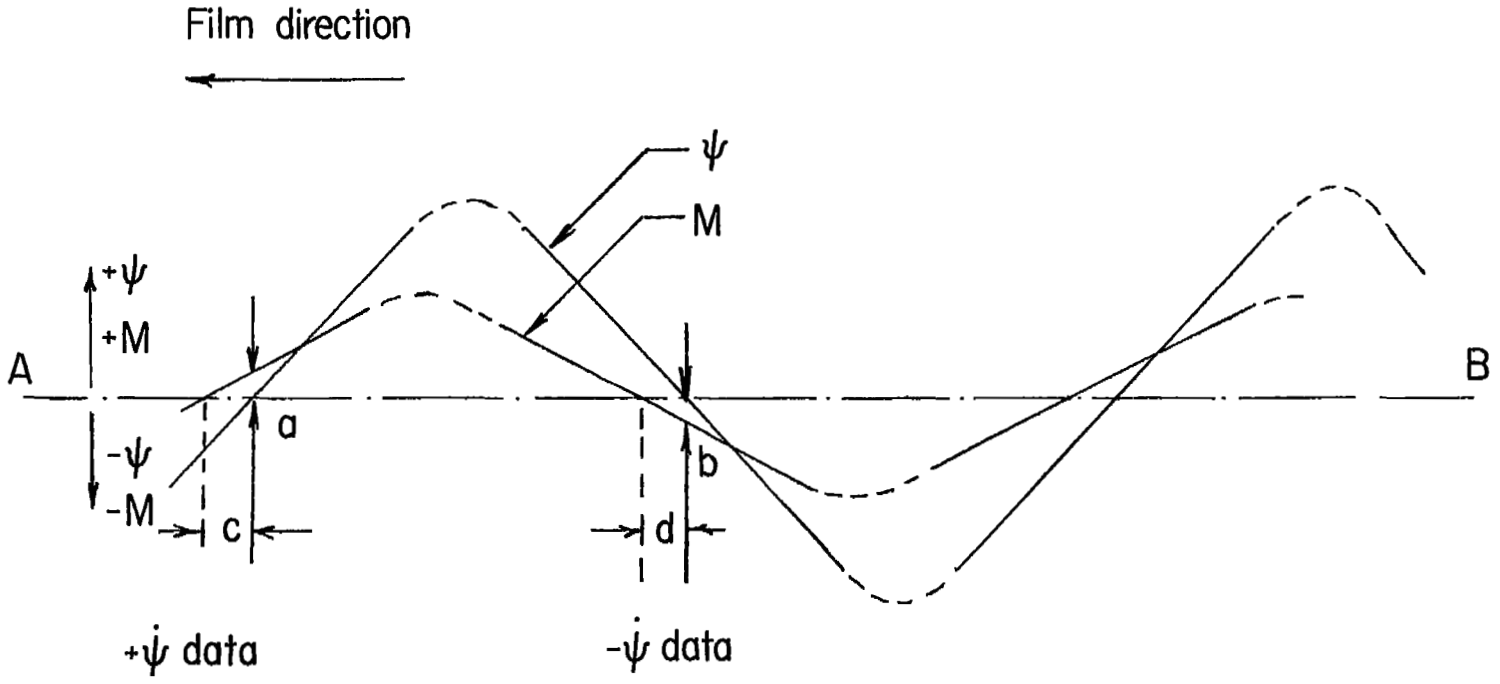

Figure 11.- Sketch of a moment and angular position trace illustrating the method of reducing the data.

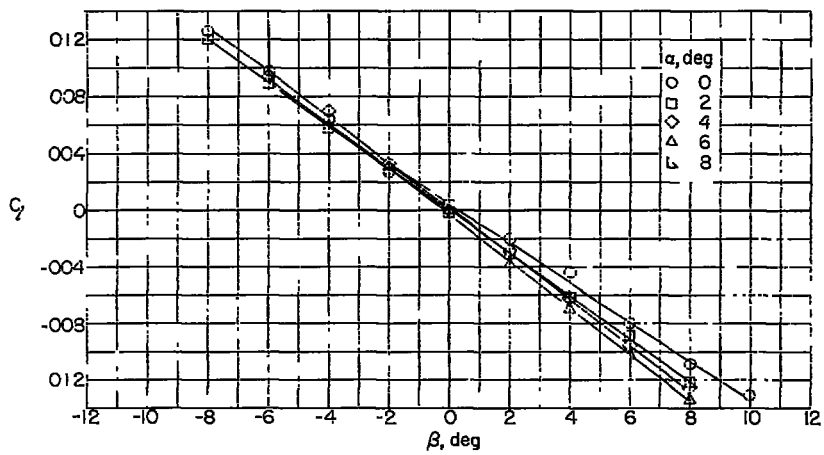

(a) Complete configuration.

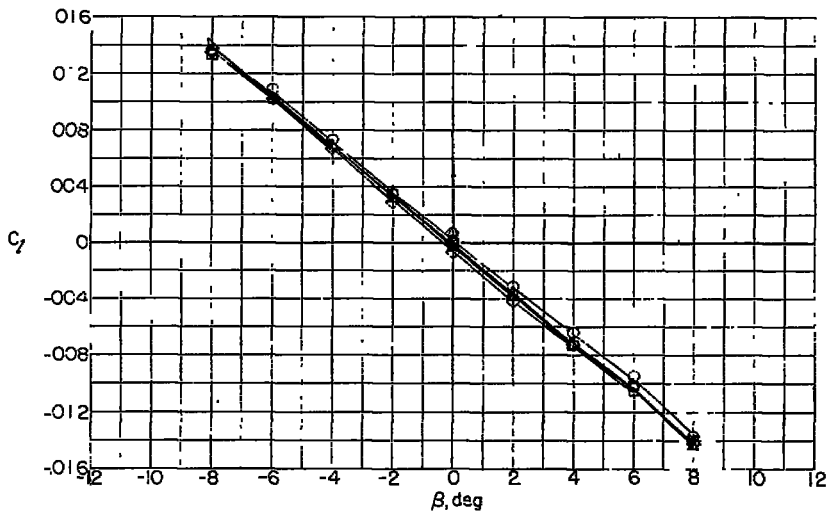

(b) Body-tail configuration.

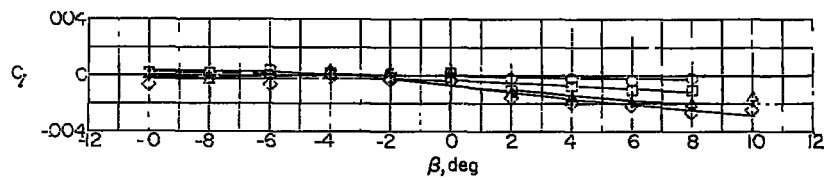

(c) Body-wing configuration.

Figure 12.- Variation of rolling-moment coefficient with sideslip angle at Mach number, 1.62. (C_l measured about body axis; β measured in stability axis.)

[redacted]

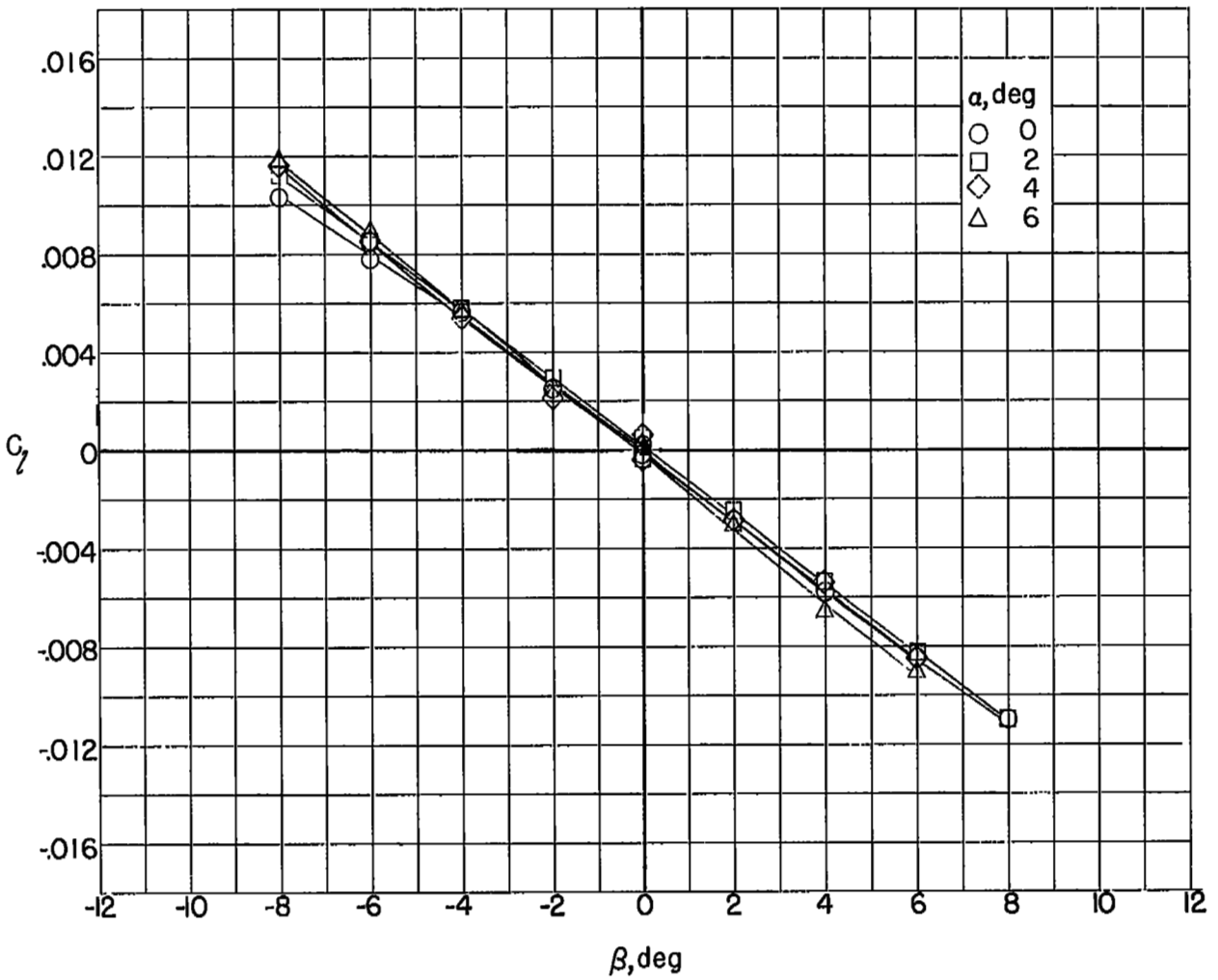

Figure 13.- Variation of rolling-moment coefficient for the complete configuration with sideslip angle at Mach number, 1.94. (C_l measured about body axis; β measured in stability axis.)

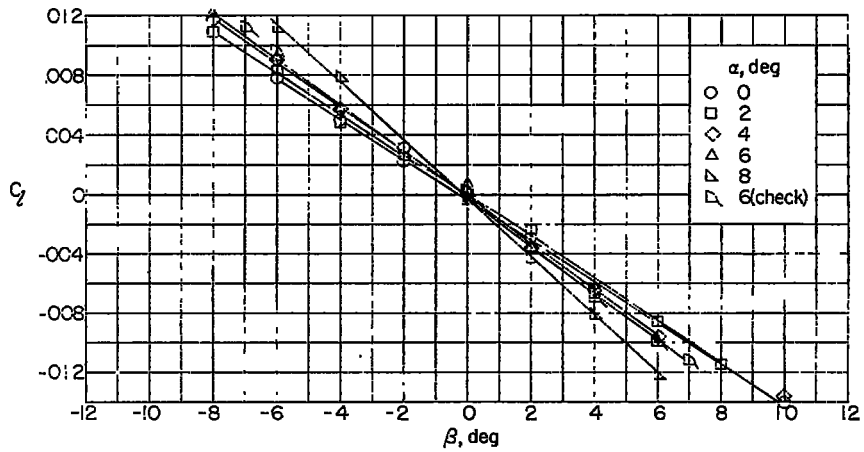

(a) Complete configuration.

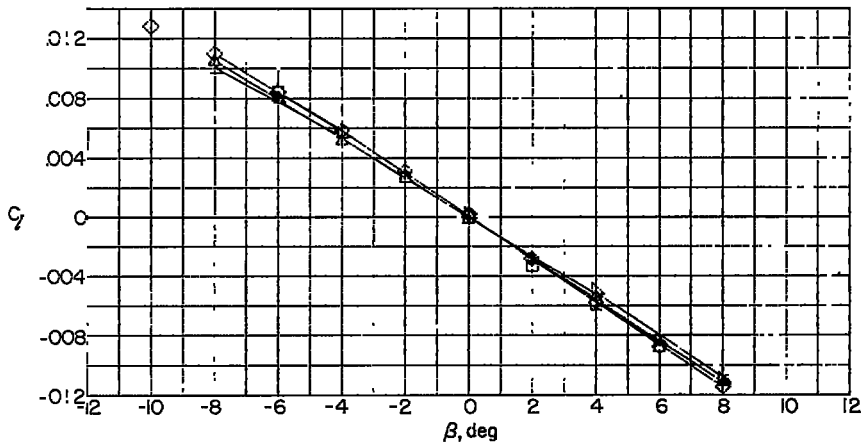

(b) Body-tail configuration.

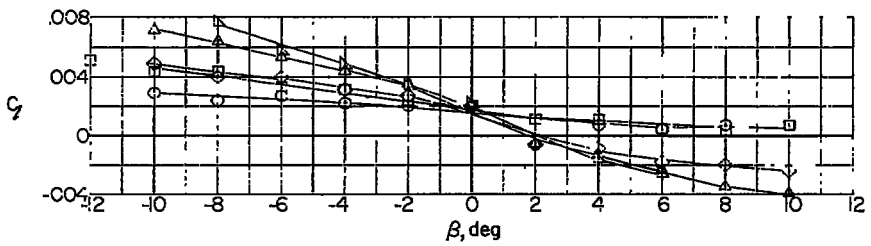

(c) Body-wing configuration.

Figure 14.- Variation of rolling-moment coefficient with sideslip angle at Mach number 2.41. (C_l measured about body axis; β measured in stability axis.)

[redacted]

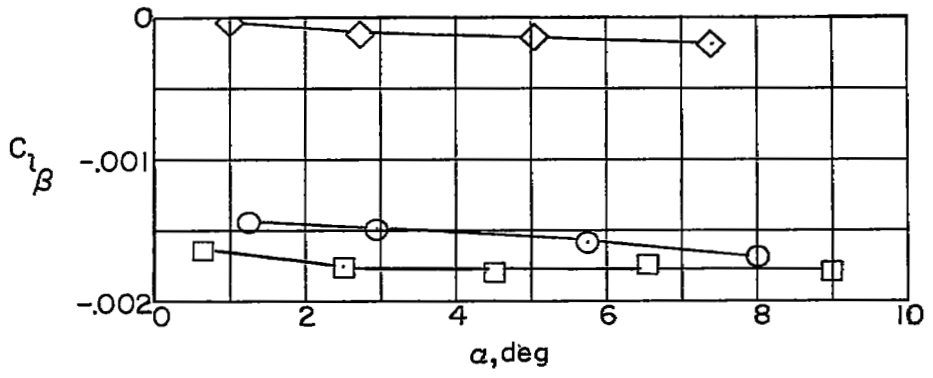

(a) M = 1.62.

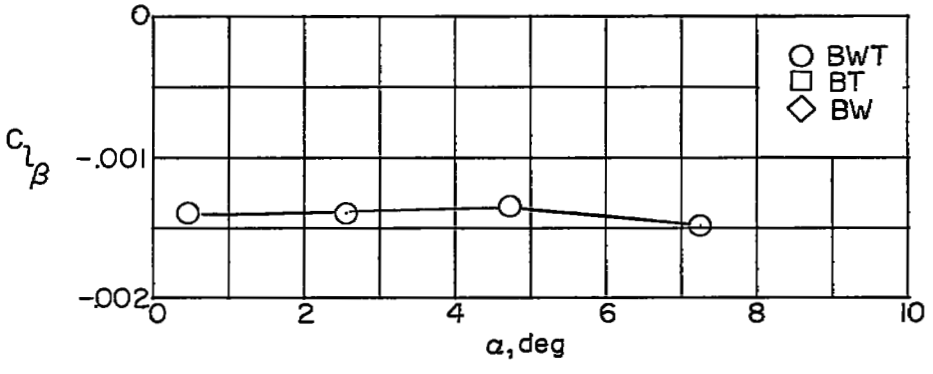

(b) M = 1.94.

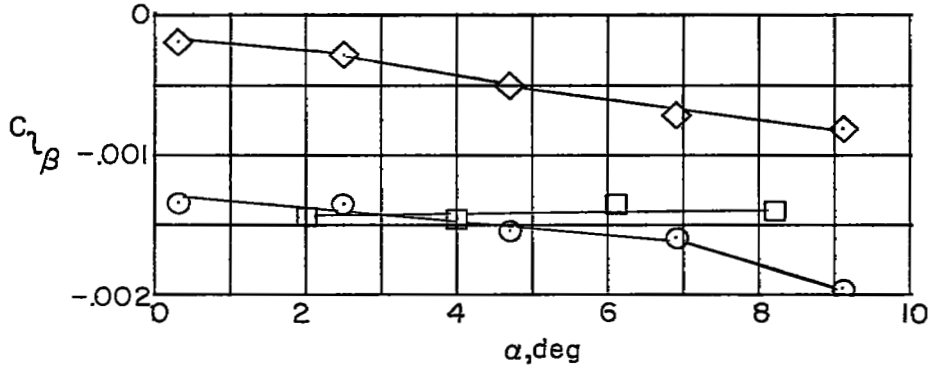

(c) M = 2.41.

Figure 15.- Variation of C_{l_β} (per degree) with angle of attack for various configurations. (C_l measured about body axis; β measured in stability axis.)

[redacted]

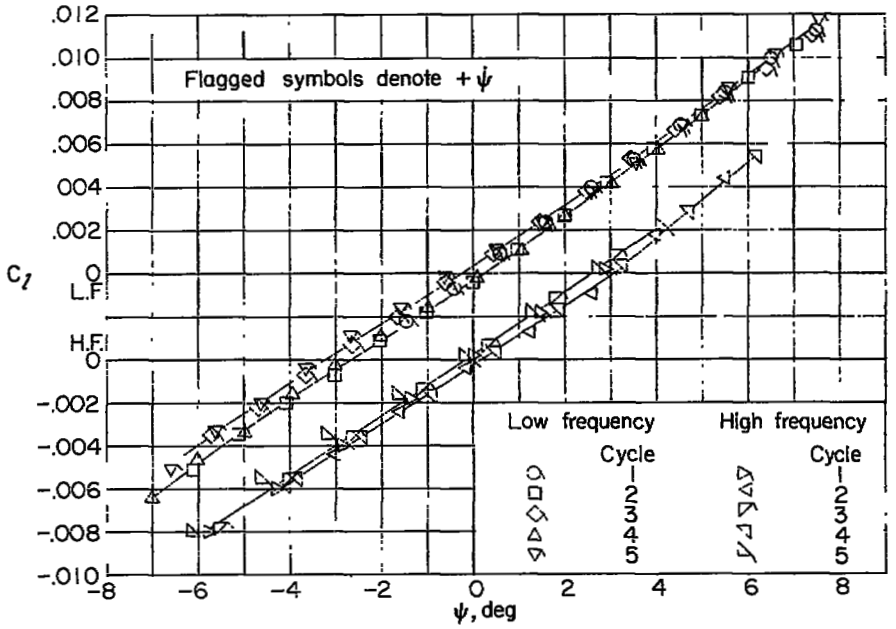

(a) $\alpha = 1.25^{\circ}$.

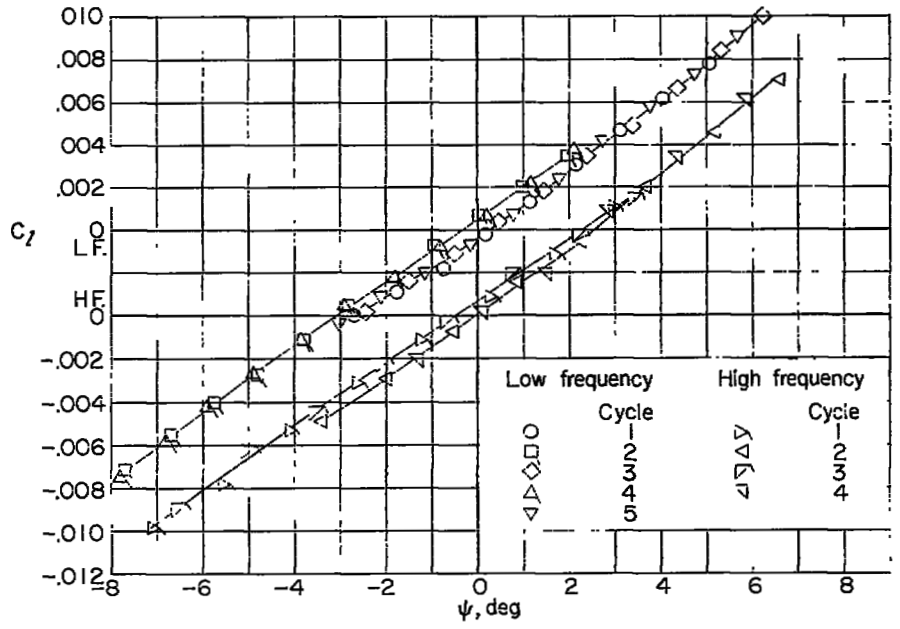

(b) $\alpha = 2.95^{\circ}$.

Figure 16.- Dynamic variation of rolling-moment coefficient with angle of yaw for the complete configuration at Mach number 1.62.

[redacted]

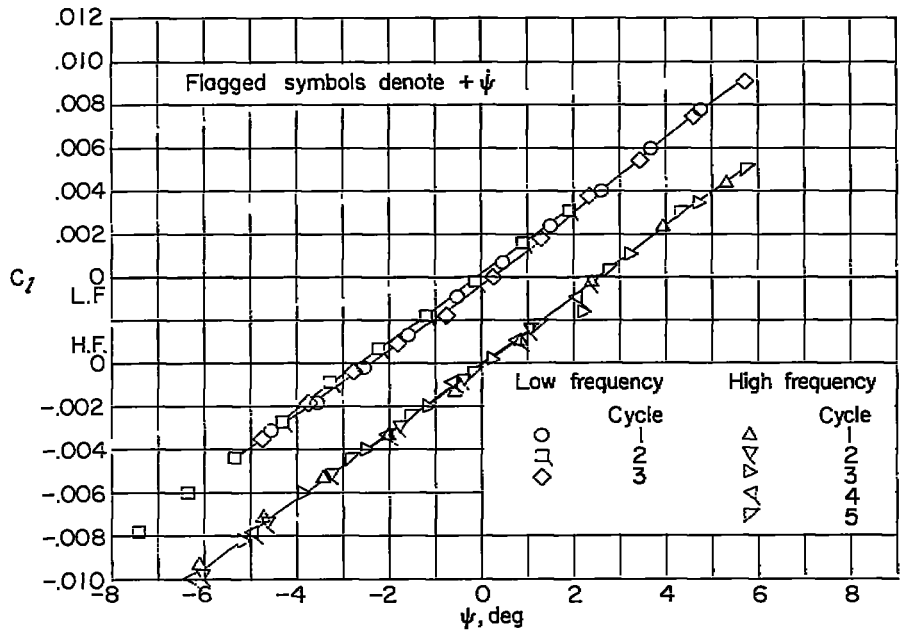

(c) $\alpha = 5.75^{\circ}$.

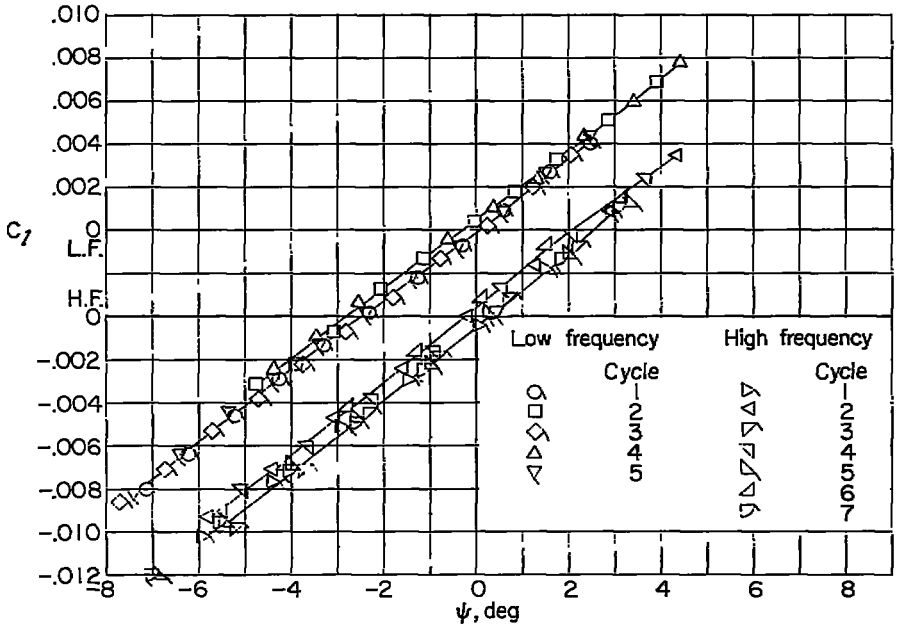

(d) $\alpha = 8.02^{\circ}$.

Figure 16.- Concluded.

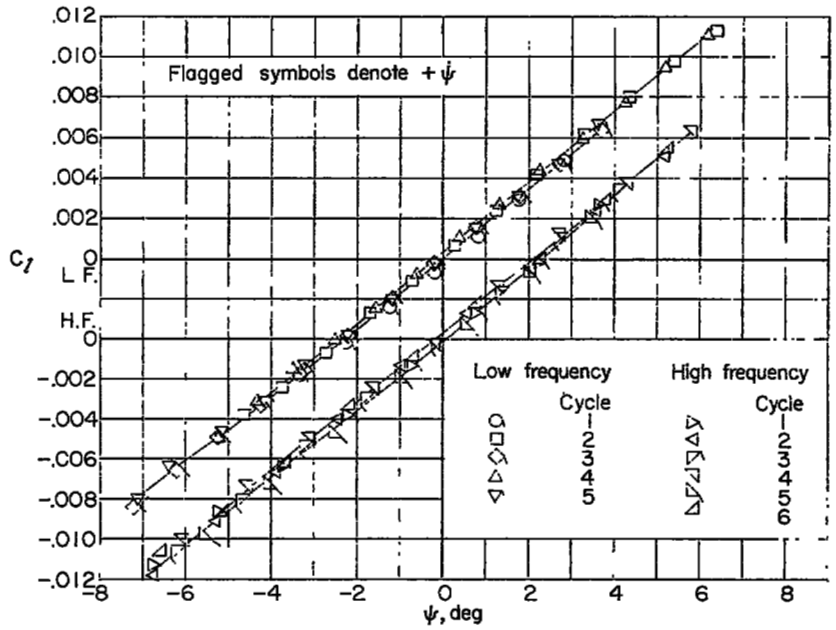

(a) $\alpha = 0.65°$.

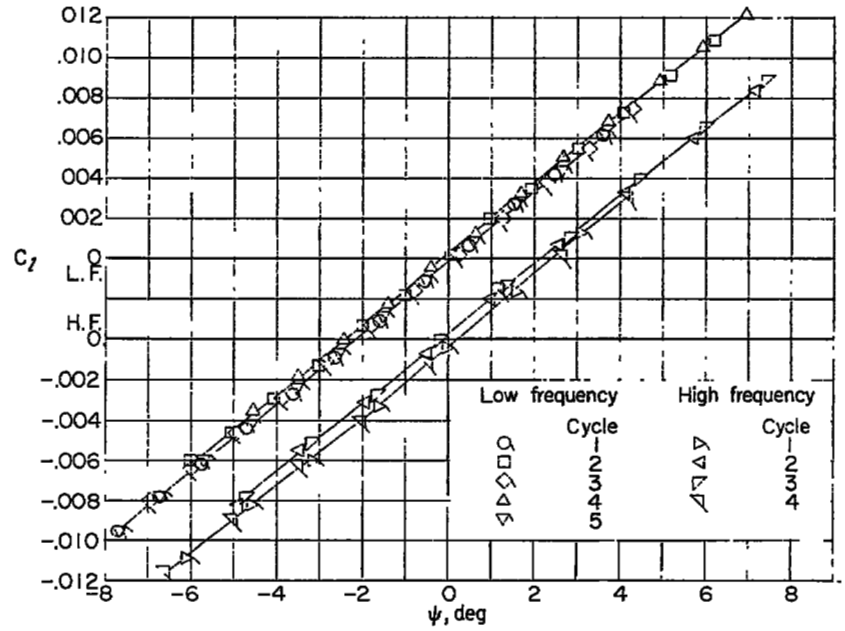

(b) $\alpha = 2.50°$.

Figure 17.- Dynamic variation of rolling-moment coefficient with angle of yaw for the body-tail configuration at Mach number 1.62.

[redacted]

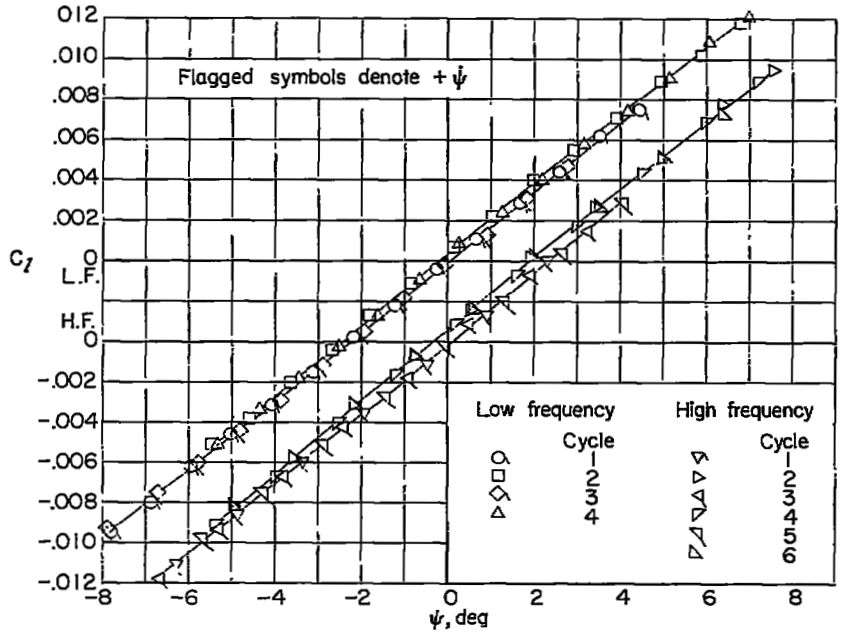

(c) $\alpha = 4.50°$.

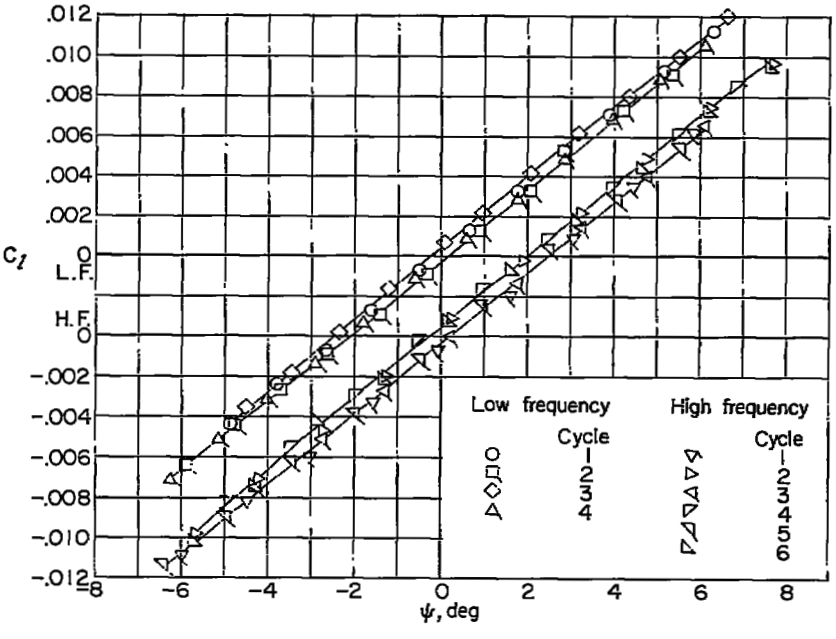

(d) $\alpha = 6.55°$.

Figure 17.- Continued.

[redacted]

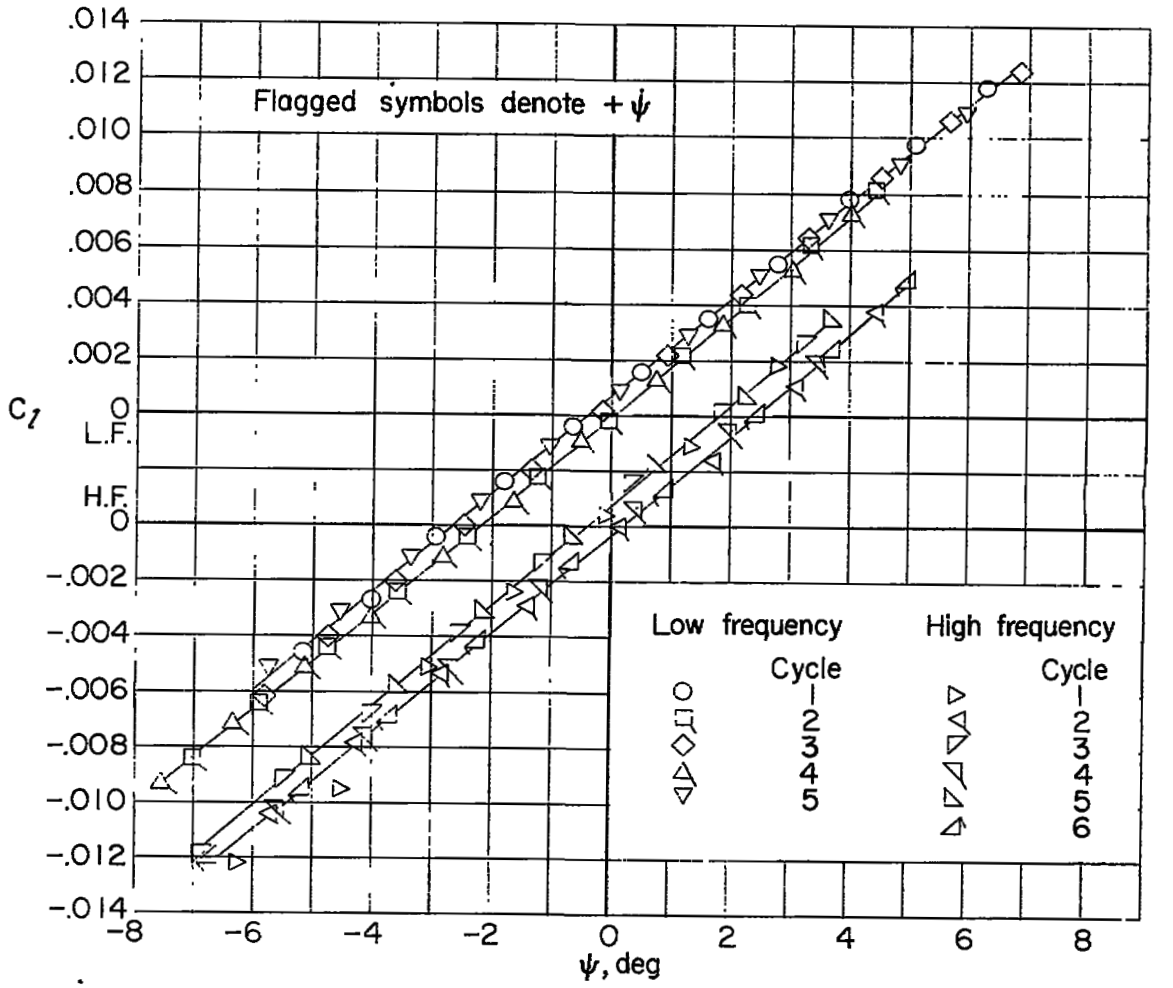

(e) $\alpha = 9.00^{\circ}$.

Figure 17.- Concluded.

[redacted]

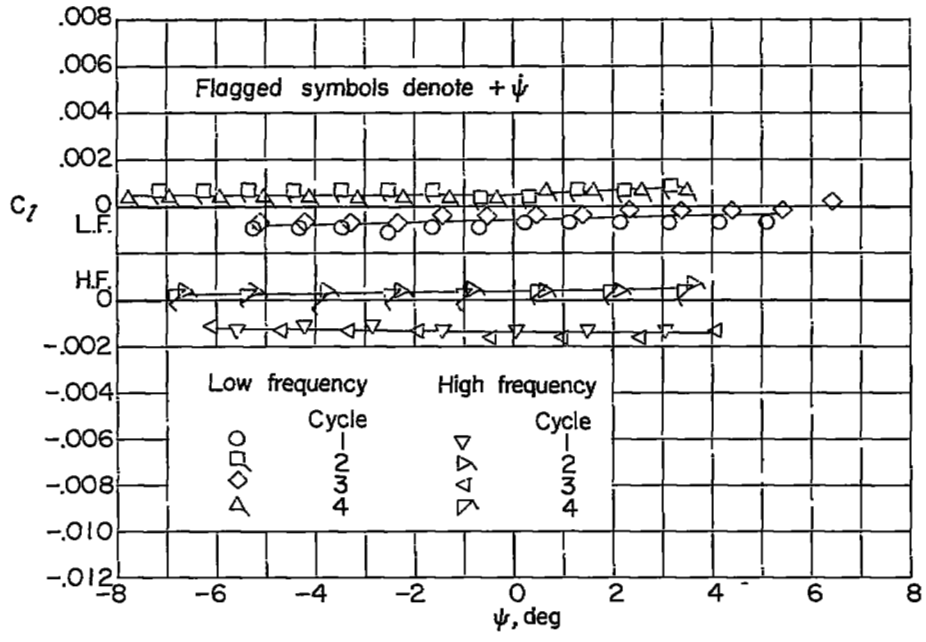

(a) $\alpha = 1.00^{\circ}$.

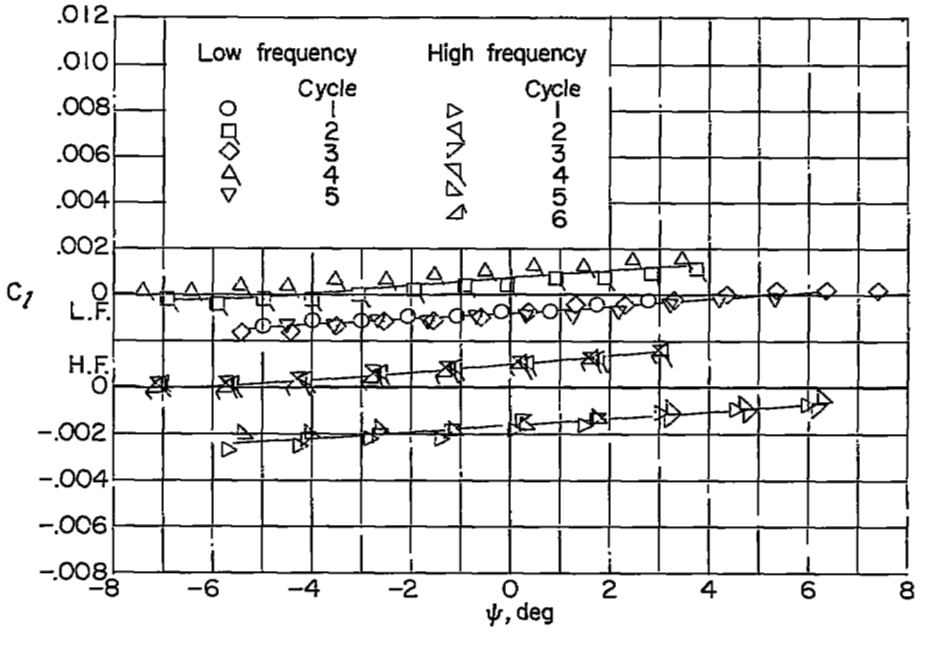

(b) $\alpha = 2.72^{\circ}$.

Figure 18.- Dynamic variation of rolling-moment coefficient with angle of yaw for the body-wing configuration at Mach number 1.62.

[redacted]

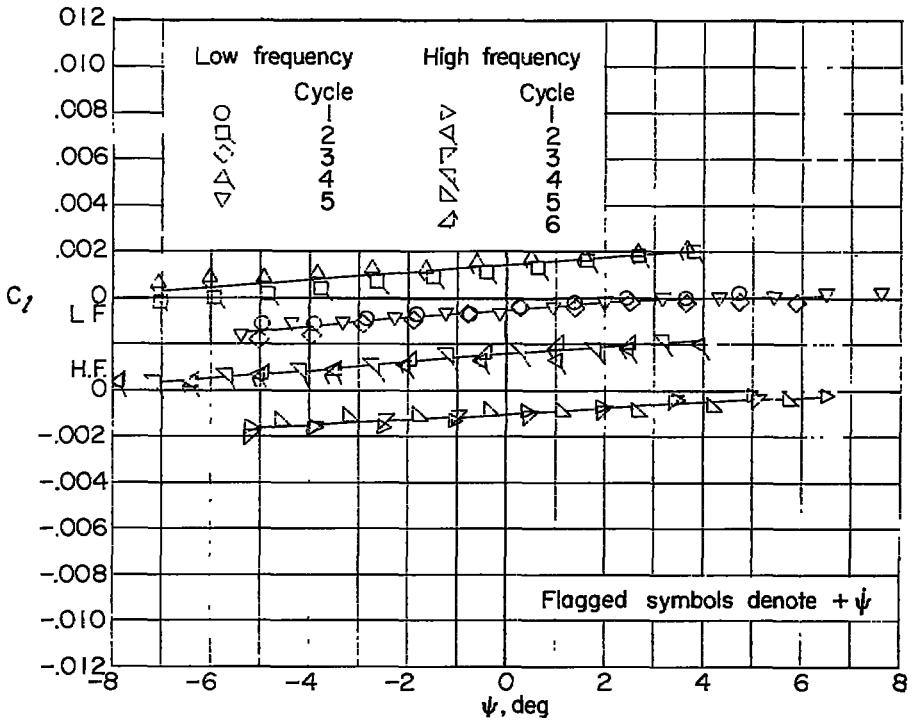

(c) $\alpha = 5.05°$.

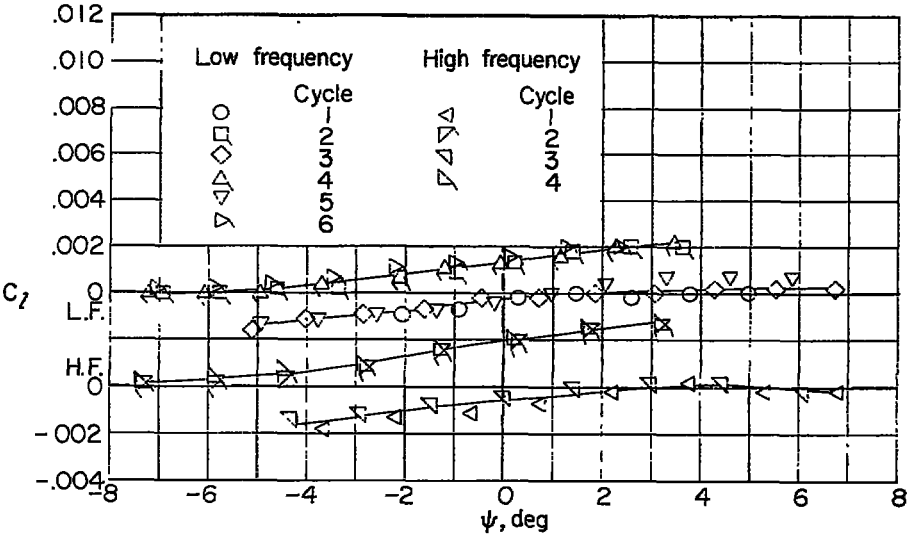

(d) $\alpha = 7.40°$.

Figure 18.- Concluded.

[redacted]

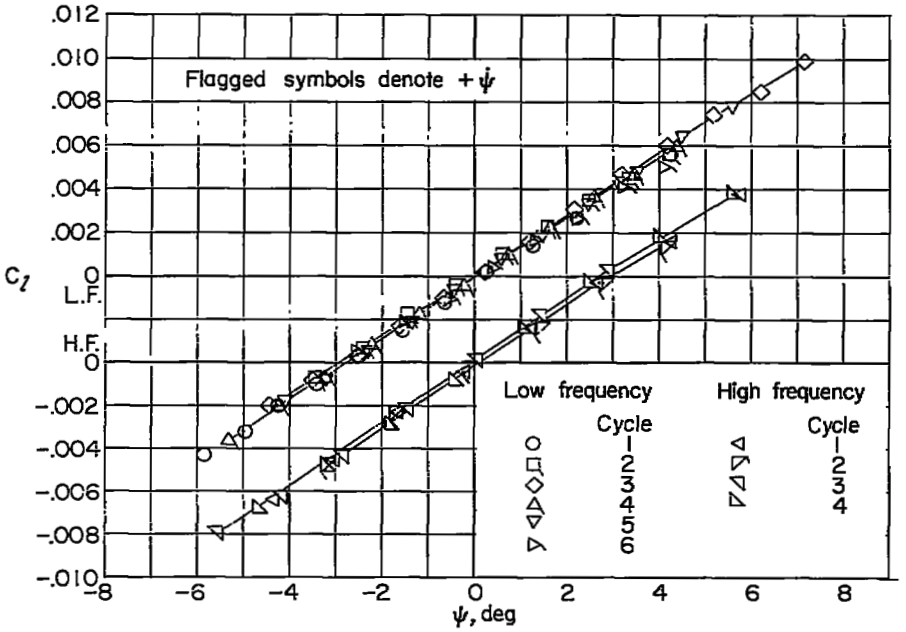

(a) $\alpha = 0.45°$.

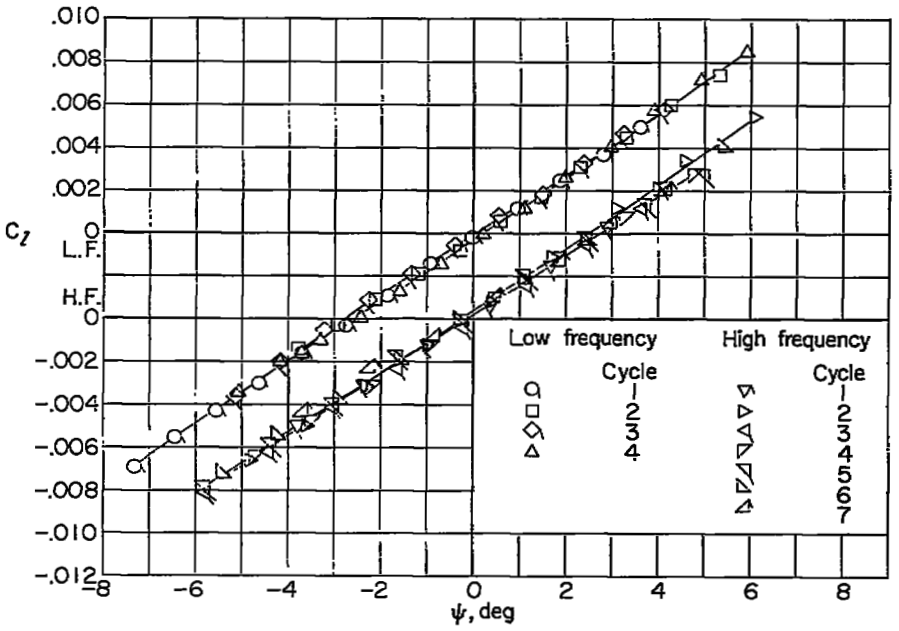

(b) $\alpha = 2.55°$.

Figure 19.- Dynamic variation of rolling-moment coefficient with angle of yaw for the complete configuration at Mach number 1.94.

[redacted]

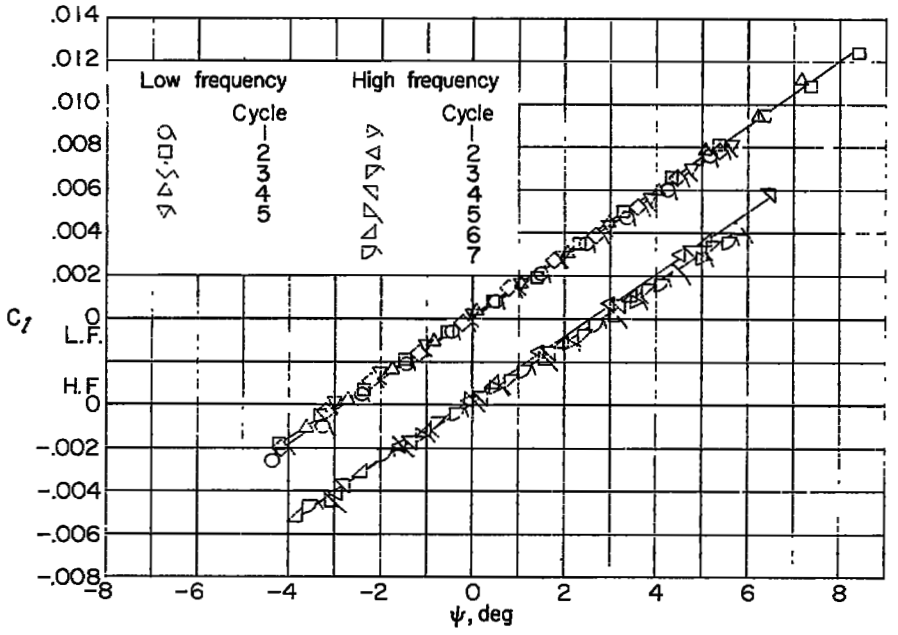

(c) $\alpha = 4.70°$.

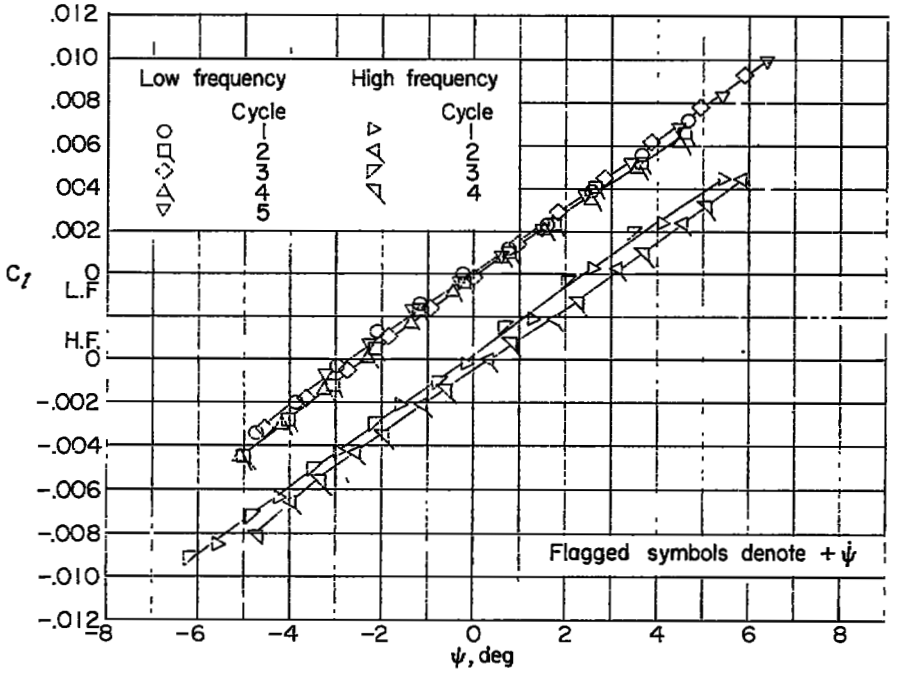

(d) $\alpha = 7.25°$.

Figure 19.- Concluded.

[redacted]

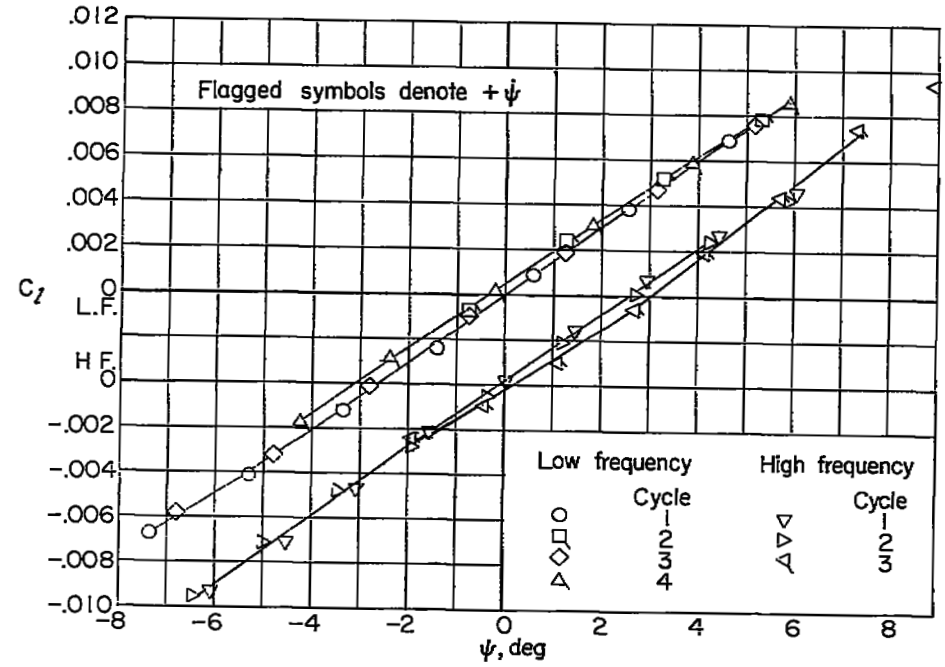

(a) $\alpha = 0.3^\circ$.

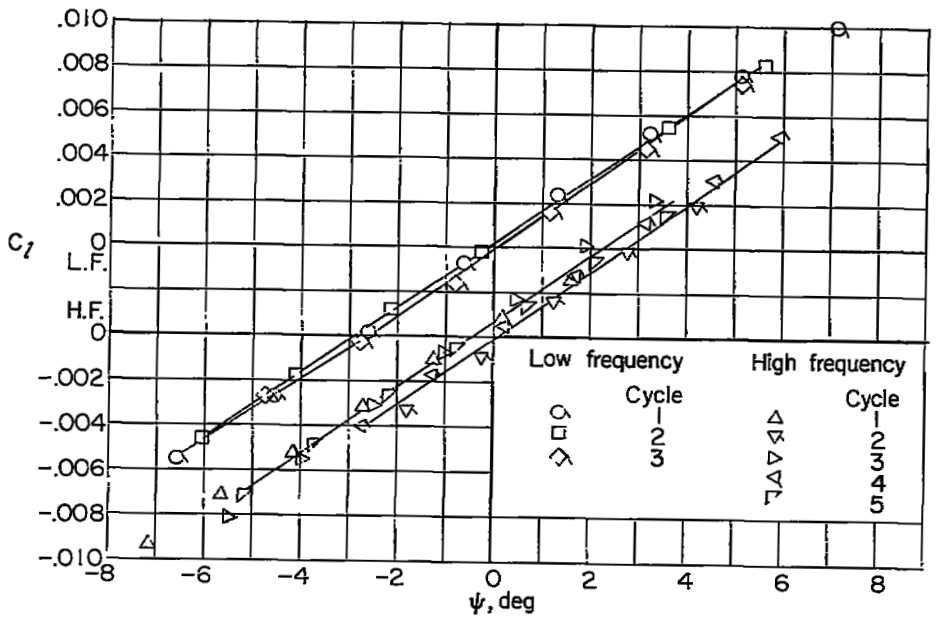

(b) $\alpha = 2.5^\circ$.

Figure 20.- Dynamic variation of rolling-moment coefficient with angle of yaw for the complete configuration at Mach number 2.41.

[redacted]

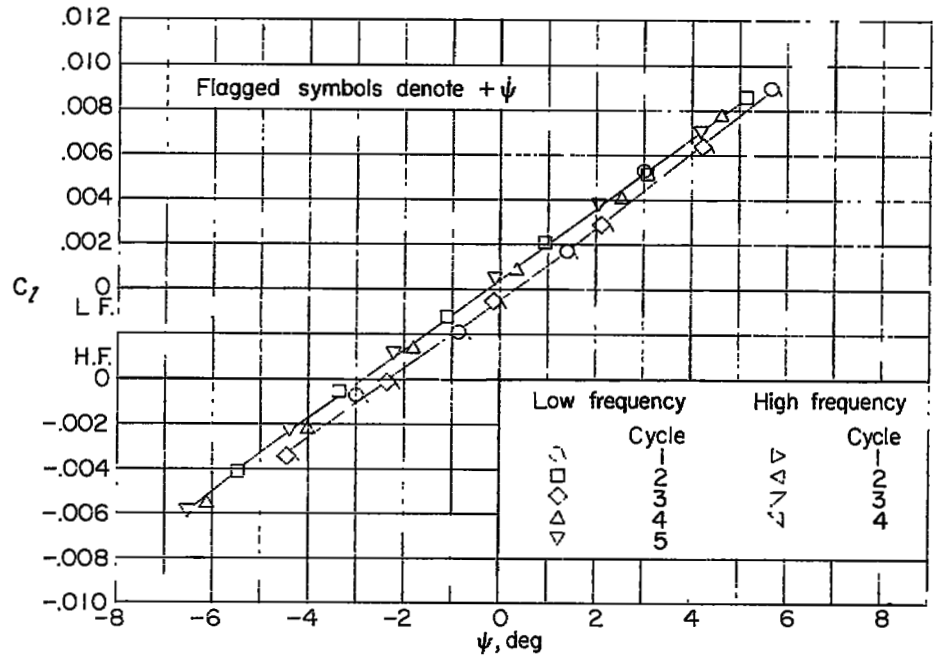

(c) $\alpha = 4.7°$.

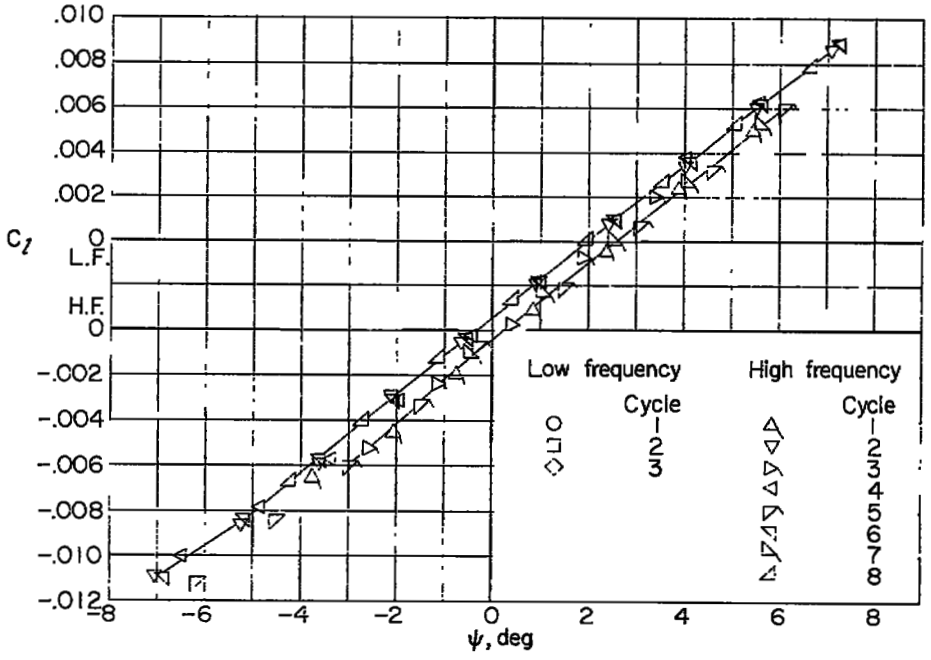

(d) $\alpha = 6.9°$.

Figure 20.- Continued.

[redacted]

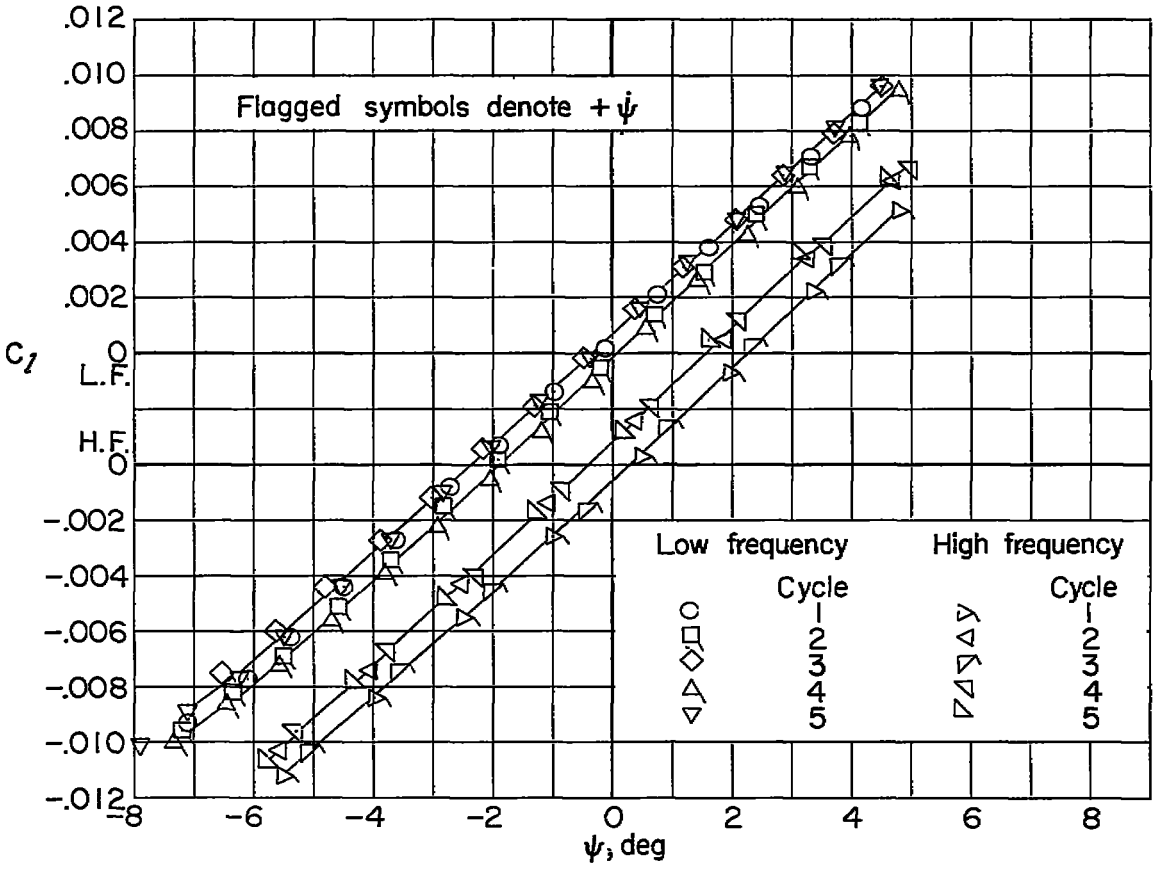

(e) $\alpha = 9.1^{\circ}$.

Figure 20.- Concluded.

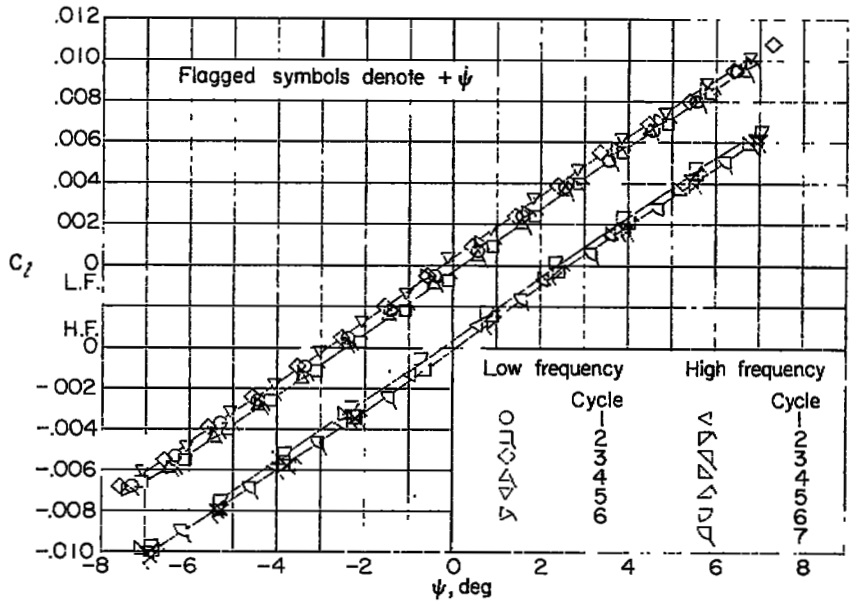

(a) $\alpha = 2.0°$.

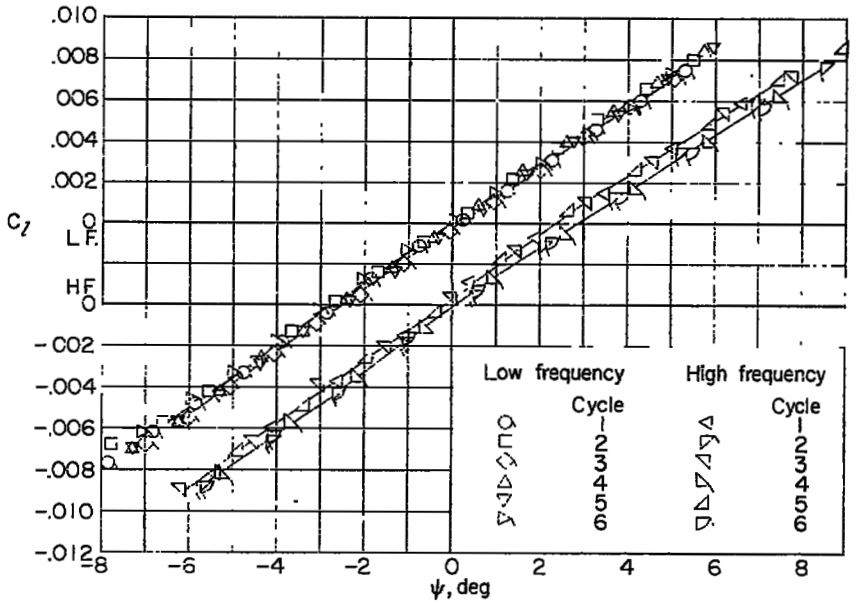

(b) $\alpha = 4.0°$.

Figure 21.- Dynamic variation of rolling-moment coefficient with angle of yaw for the body-tail configuration at Mach number 2.41.

[redacted]

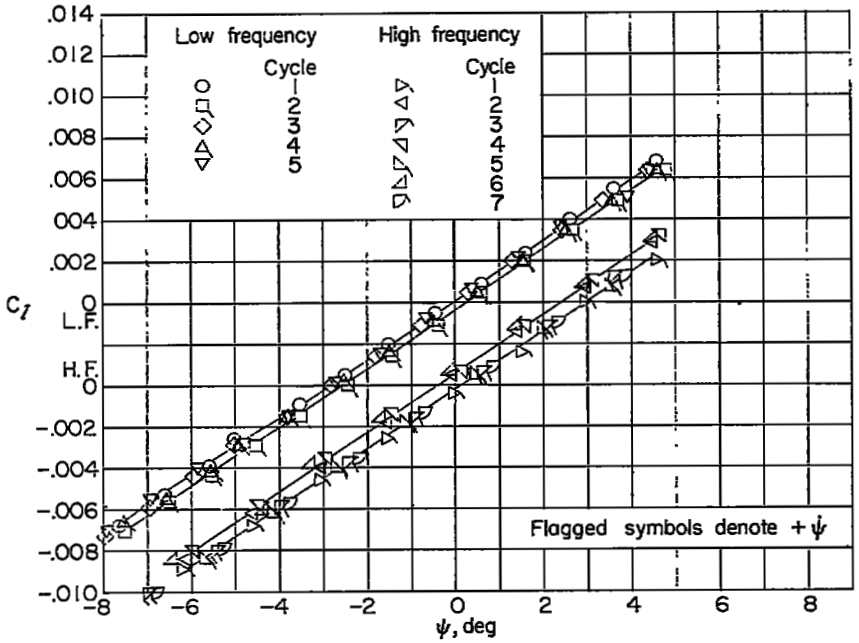

(c) $\alpha = 6.1^\circ$.

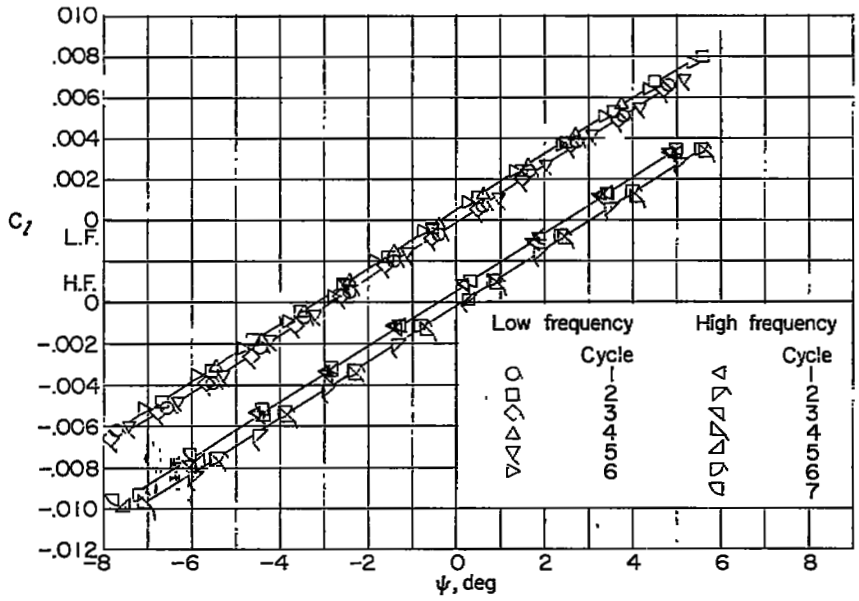

(d) $\alpha = 8.2^\circ$.

Figure 21.- Concluded.

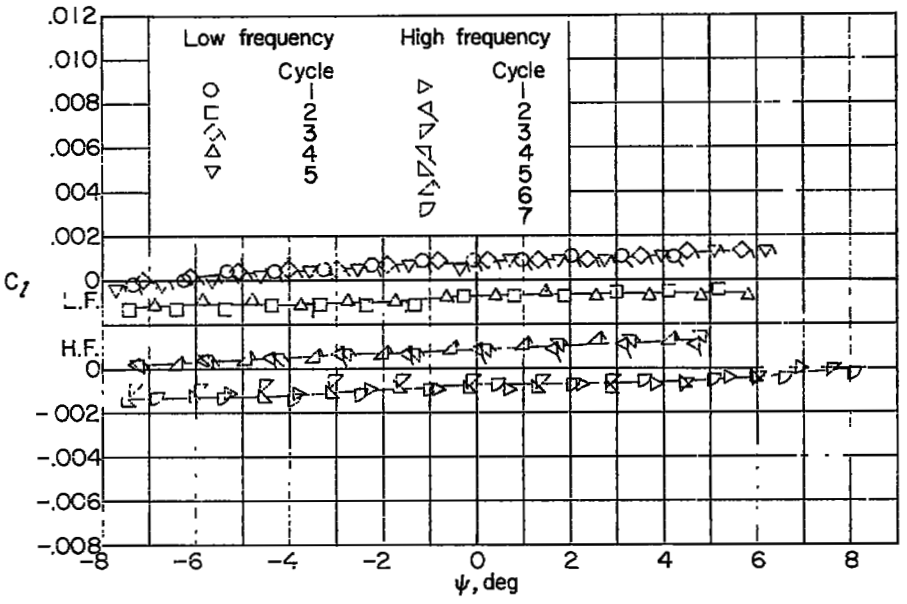

(a) $\alpha = 0.3°$.

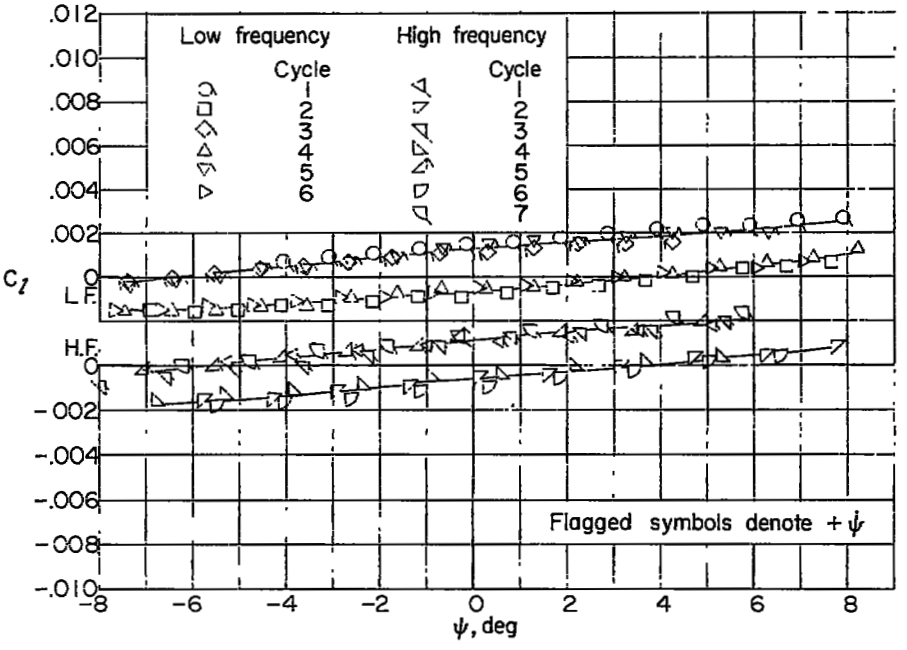

(b) $\alpha = 2.5°$.

Figure 22.- Dynamic variation of rolling-moment coefficient with angle of yaw for the body-wing configuration at Mach number 2.41.

[redacted]

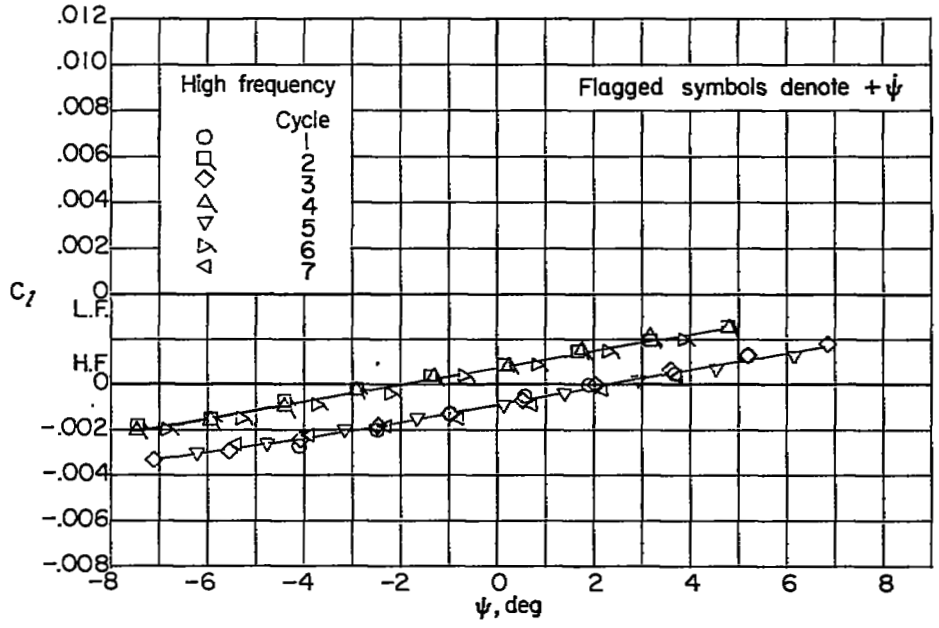

(c) $\alpha = 4.7^\circ$.

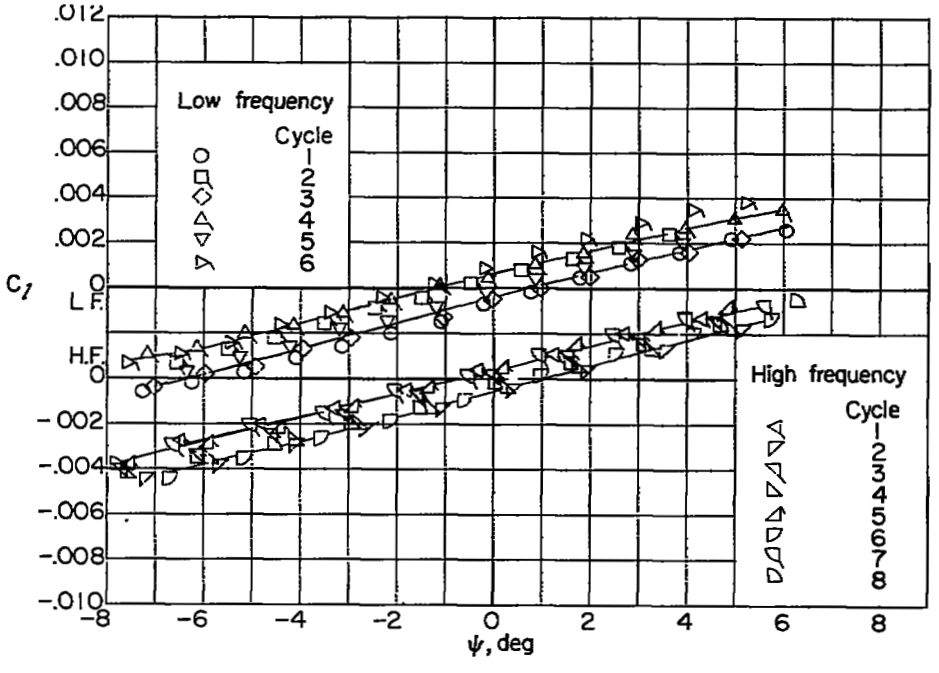

(d) $\alpha = 6.9^\circ$.

Figure 22.- Continued.

[redacted]

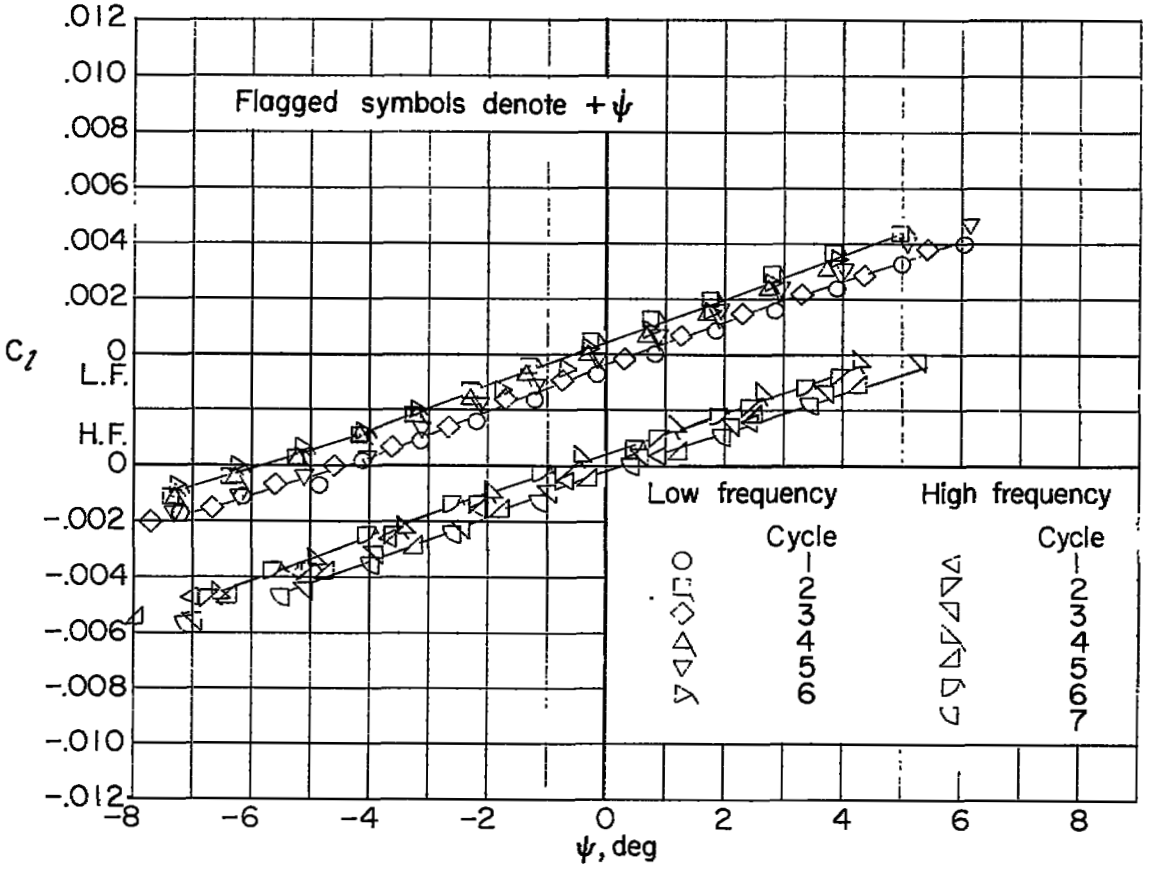

(e) $\alpha = 9.1^\circ$.

Figure 22.- Concluded.

[redacted]

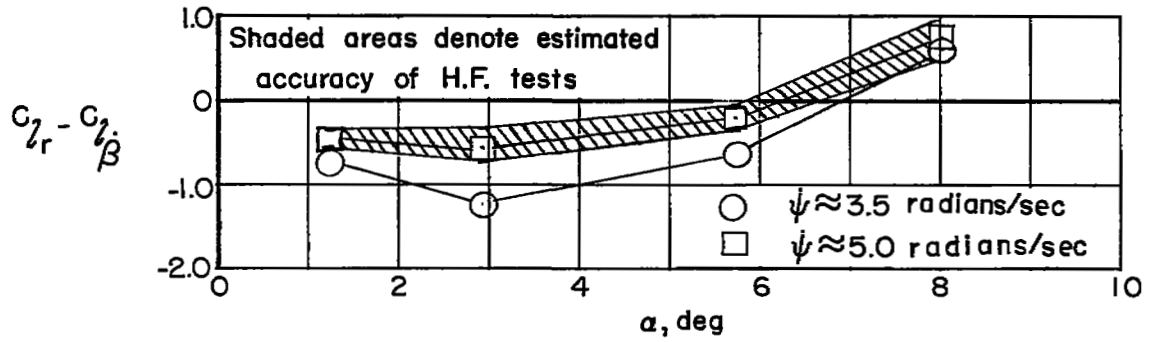

(a) Complete configuration.

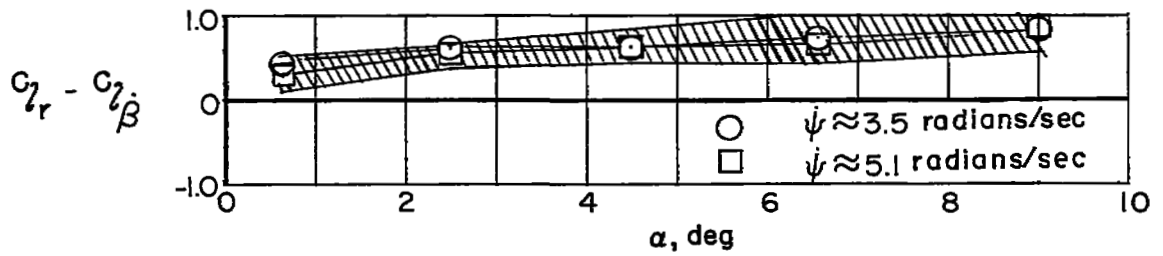

(b) Body-tail configuration.

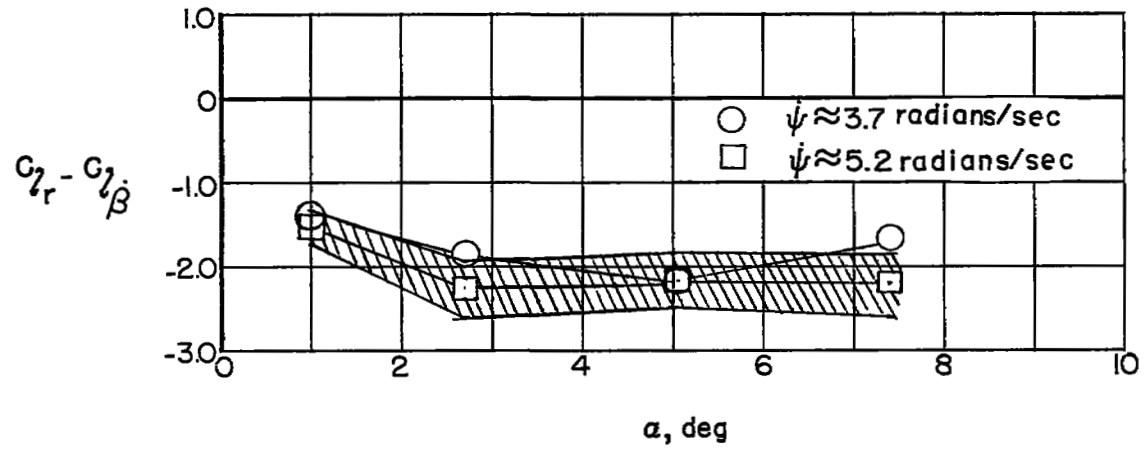

(c) Body-wing configuration.

Figure 23.- Variation of the cross derivative $C_{l_r} - C_{l_{\dot{\beta}}}$ with angle of attack and frequency at Mach number 1.62.

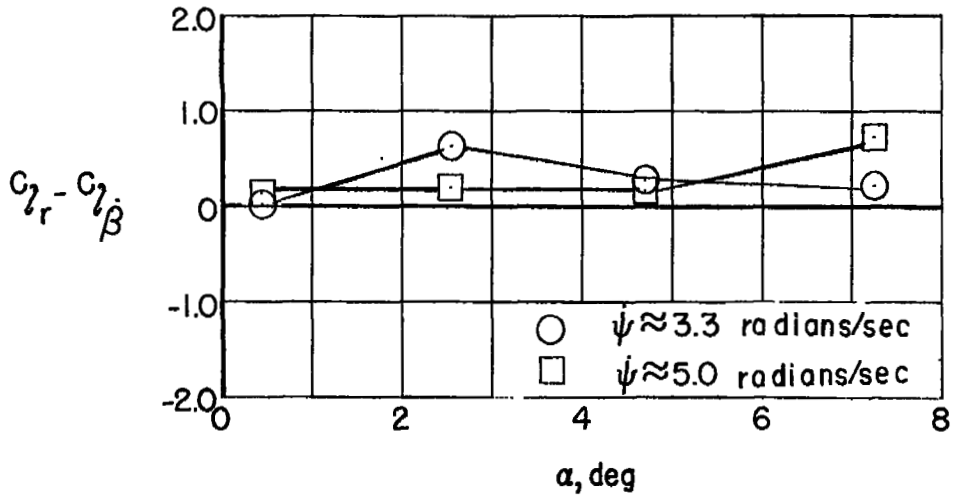

Figure 24.- Variation of the cross derivative $C_{l_r} - C_{l_{\dot{\beta}}}$ with angle of attack and frequency for the complete configuration at Mach number 1.94.

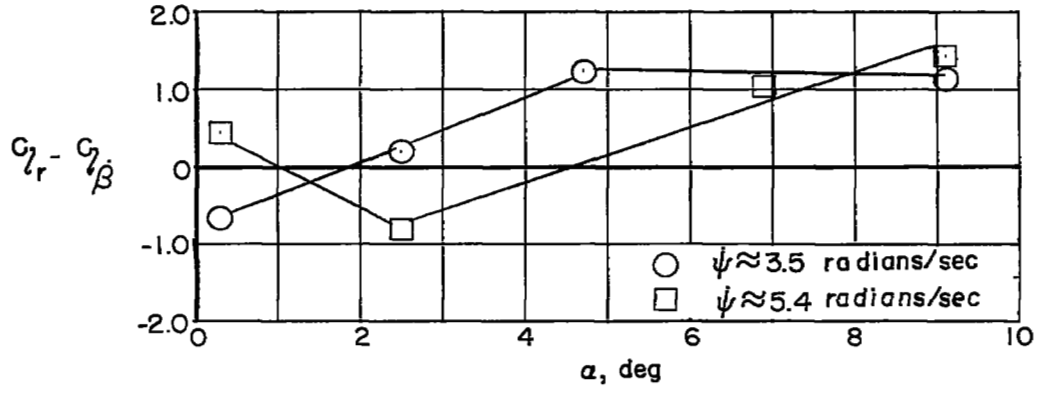

(a) Complete configuration.

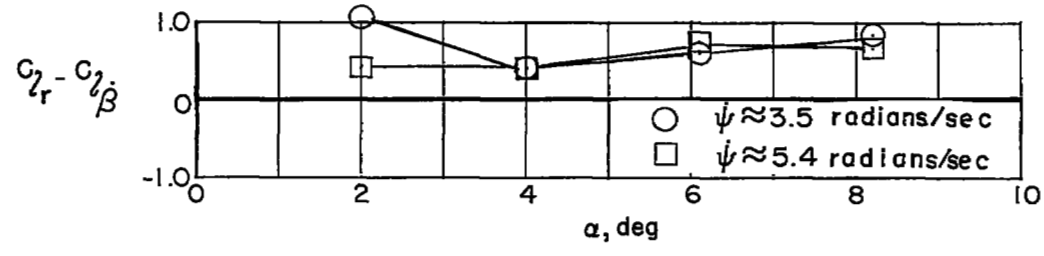

(b) Body-tail configuration.

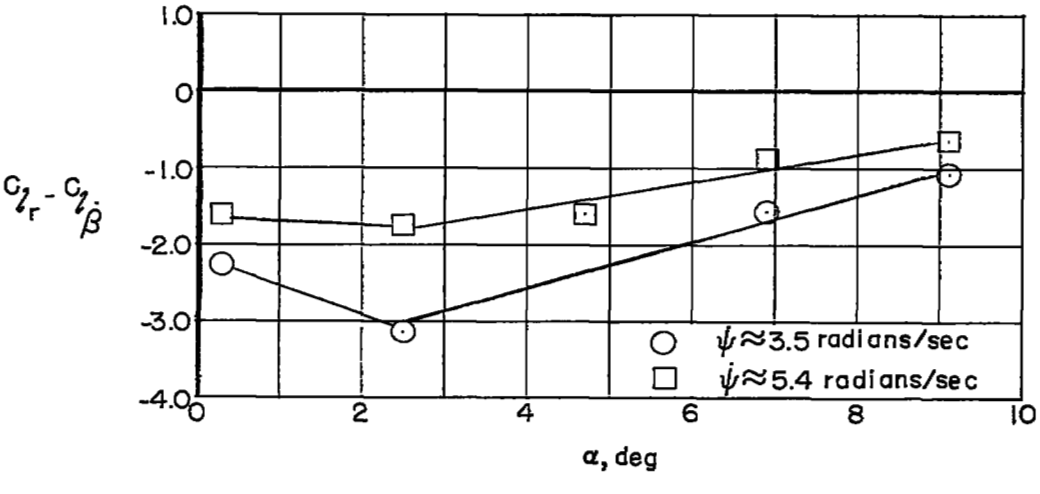

(c) Body-wing configuration.

Figure 25.- Variation of the cross derivative $C_{l_r} - C_{l_{\dot{\beta}}}$ with angle of attack and frequency at Mach number 2.41.